

The Host Galaxies and Classification of Active Galactic Nuclei

Lisa J. Kewley¹★

University of Hawaii, 2680 Woodlawn Drive, Honolulu, HI 96822, USA

Brent Groves, Guinevere Kauffmann

Max Plank Institut fur Astrophysik

Tim Heckman

Johns Hopkins University

Submitted 2006 May 26

ABSTRACT

We present an analysis of the host properties of 85224 emission-line galaxies selected from the Sloan Digital Sky Survey. We show that Seyferts and LINERs form clearly separated branches on the standard optical diagnostic diagrams. We derive a new empirical classification scheme which cleanly separates star-forming galaxies, composite AGN-H II galaxies, Seyferts and LINERs and we study the host galaxy properties of these different classes of objects. LINERs are older, more massive, less dusty and more concentrated, and they and have higher velocity dispersions and lower [OIII] luminosities than Seyfert galaxies. Seyferts and LINERs are most strongly distinguished by their [OIII] luminosities. We then consider the quantity $L[\text{OIII}]/\sigma^4$, which is an indicator of the black hole accretion rate relative to the Eddington rate. Remarkably, we find that at *fixed* $L[\text{OIII}]/\sigma^4$, all differences between Seyfert and LINER host properties disappear. LINERs and Seyferts form a continuous sequence, with LINERs dominant at low L/L_{EDD} and Seyferts dominant at high L/L_{EDD} . These results suggest that the majority of LINERs are AGN and that the Seyfert/LINER dichotomy is analogous to the high/low-state transition for X-ray binary systems. We apply theoretical photo-ionization models and show that pure LINERs require a harder ionizing radiation field with lower ionization parameter than Seyfert galaxies, consistent with the low and high X-ray binary states.

1 INTRODUCTION

The majority of nearby AGN and AGN candidates have nuclear optical spectra that are dominated by emission lines of low ionization species such as [OI] $\lambda 6300$, [O II] $\lambda\lambda 3726, 9$ and [S II] $\lambda\lambda 6717, 31$ (Ho et al. 1997b). This class of AGN was first defined by Heckman (1980) as LINERs (Low Ionization Narrow Emission-line Regions). LINERs have lower luminosities than Seyfert galaxies or quasars and are therefore often referred to as low-luminosity active galactic nuclei (LLAGN). LINER emission is extremely common in the nuclei of galaxies; up to $\sim 1/3$ of all galaxies have nuclear spectra typical of LINERs (Heckman 1980; Ho et al. 1995, 1997). Despite the prevalence of LINERs in galaxies and decades of study, the power source of LINERs is still under debate. Some LINER galaxies have double-peaked broad Balmer lines (Eracleous & Halpern 2001; Storchi-Bergmann et al.

1997; Bower et al. 1996), while others have compact radio cores (Falcke et al. 2000; Ulvestad & Ho 2001; Filho et al. 2002, 2004; Anderson et al. 2004), evidence for hard X-ray spectra (Terashima et al. 2000; Ho et al. 2001), and/or UV variability (Maoz et al. 2005). These observations provide circumstantial evidence for an AGN power source for the LINER emission. Other possible power sources include fast shocks (Heckman 1980; Dopita & Sutherland 1995; Lípari et al. 2004), photoionization by hot stars (Filippenko & Terlevich 1992; Shields 1992; Maoz et al. 1998; Barth & Shields 2000), or photoionization by an old, metal-rich stellar population (Taniguchi et al. 2000; Alonso-Herrero et al. 2000). LINER emission has been observed in extranuclear regions associated with large-scale outflows and related shocks (Lípari et al. 2004), or regions shocked by radio jets (Cecil et al. 2000).

Recent investigations into the stellar populations of LINER host galaxies have yielded important insight into their nature. Maoz et al. (1998) and Colina et al. (2002) de-

★ Hubble Fellow; kewley@ifa.hawaii.edu

tected stellar wind lines in UV spectra of weak [O I]/H α LINERs. Similar features have been detected in some Seyfert galaxies from nuclear starbursts that are a few Myr old (Heckman et al. 1997; González Delgado et al. 1998). González Delgado et al. (2004) searched the HST STIS spectra of 28 LINERs for Wolf-Rayet features. They found no Wolf-Rayet features and little evidence of young stars in LINERs with strong [O I]/H α . In LINERs with low [O I]/H α intermediate-age stars contribute significantly to the stellar continuum. Fernandes et al. (2004) found that while massive stars do not contribute significantly to LINER spectra, high order Balmer absorption lines are detected in $\sim 50\%$ of LINERs that have relatively weak [O I] $\lambda 6300$ emission. These results indicate that the current LINER classification scheme encompasses two or more types of galaxies, or galaxies at different stages in evolution.

LINERs are commonly classified using their optical emission-line ratios. The first optical classification classification scheme to segregate LINERs from other spectral types was proposed by Heckman (1980). This scheme uses line ratios of the low ionization species [O I] $\lambda 6300$ and [O II] $\lambda\lambda 3726, 29$ compared to the high ionization species [O III] $\lambda 5007$ to separate LINERs from Seyferts. This scheme requires the use of additional diagnostics to remove star-forming galaxies. The most common method to remove star-forming galaxies is based on the Baldwin et al. (1981) empirical diagnostic diagrams using the optical line ratios [O I]/H α , [S II]/H α , [N II]/H α , and [O III]/H β . The Baldwin et al. scheme was revised by Osterbrock & Pogge (1985) and Veilleux & Osterbrock (1987). An alternative scheme was proposed by Ho et al. (1997) that includes an additional division between “pure” LINERs and LINER/H II “transition” objects using the [O I]/H α ratio. Transition objects have line ratios that are intermediate between the two classes. This division is arbitrary because there was no clear division in [O I]/H α between transition or true LINER classes. The first purely theoretical classification scheme to distinguish between AGN, LINERs, and H II region-like objects was derived by Kewley et al. (2001b). They used a combination of modern stellar population synthesis, photoionization, and shock models to derive a “maximum starburst line” and an “extreme mixing line” for separation of the three types of objects. Kewley et al. concluded that previous LINER classification schemes include starburst-Seyfert composites in the LINERs class, as well as bona-fide LINERs. Recently, Kauffmann et al. (2003a) shifted the Kewley et al. extreme starburst line to make a semi-empirical fit to the outer bound of $\sim 22,600$ SDSS spectra. This outer bound defines the region where composite starburst-AGN objects are expected to lie on the diagnostic diagrams.

Although much progress has been made in the optical classification of the ionizing source in galaxies, none of these classification schemes has been able to divide cleanly between Seyfert, LINER and composite/transition types. The primary reason for this problem is the lack of a sufficiently large sample in which empirical boundaries between the different galaxy classes can be observed. In this paper, we use 85,224 galaxies from the Sloan Digital Sky Survey (SDSS) data release 4 (DR4) emission-line catalog (described in Section 2) to develop a new semi-empirical classification scheme for Seyferts, LINERs, and composite objects (Section 3). We use this new classification scheme to investigate the host

properties of AGN in Section 5. Our results are discussed in Section 7 and we present our conclusions in Section 8.

Throughout this paper, we adopt the flat Λ -dominated cosmology as measured by the WMAP experiment ($h = 0.72$, $\Omega_m = 0.29$; Spergel et al. 2003).

2 SAMPLE SELECTION

Our sample was selected from the 567486-galaxy DR4 sample according to the following criteria:

- (i) Signal-to-noise ratio $S/N \geq 3$ in the strong emission-lines H β , O III $\lambda 5007$, H α , [N II] $\lambda 6584$, and [S II] $\lambda\lambda 6717, 31$.
- (ii) Redshifts between $0.04 < z < 0.1$.

The S/N criterion is required for accurate classification of the galaxies into star forming or AGN dominated classes (e.g., Kewley et al. 2001a; Veilleux & Osterbrock 1987). Our lower redshift limit ensures that the galaxy properties derived from the fiber spectra are not dominated by the small fixed-size aperture. Kewley et al. (2005) analysed the effect of a fixed size aperture on metallicity, star-formation rate, and reddening. They concluded that a minimum aperture covering fraction of $\sim 20\%$ is required for the spectral properties within the aperture to approximate the global values. For the 3'' fiber aperture of the SDSS, a 20% covering fraction corresponds roughly to a redshift of $z \sim 0.04$. Our upper redshift limit avoids incompleteness in the LINER class. LINERs typically have lower luminosities than Seyfert galaxies, and are therefore found at lower redshifts than Seyferts in the magnitude-limited SDSS survey. We will investigate incompleteness as a function of galaxy type in Section 3.1

The resulting sample contains 85224 emission-line galaxies and does not include duplicates found in the original DR4 catalog. We use the publically available emission-line fluxes (described in Tremonti et al. 2004). These fluxes were calculated using a sophisticated technique that applies a least-squares fit of stellar population synthesis models and dust attenuation to the continuum. Once the continuum has been removed, the emission-line fluxes were fit with Gaussians, constraining the width and velocity separation of the Balmer lines together, and similarly for the forbidden lines.

We have corrected the emission-line fluxes for extinction using the Balmer decrement and the Cardelli et al. (1989) reddening curve. We assume an $R_V = A_V/E(B-V) = 3.1$ and an intrinsic H α /H β ratio of 2.85 for galaxies dominated by star formation and H α /H $\beta = 3.1$ for galaxies dominated by AGN (the Balmer decrement for case B recombination at $T = 10^4$ K and $n_e \sim 10^2 - 10^4$ cm $^{-3}$; Osterbrock 1989). A total of 5414 (6%) of galaxies in our sample have Balmer decrements less than the theoretical value. A Balmer decrement less than the theoretical value can result from one or a combination of (1) intrinsically low reddening, (2) errors in the stellar absorption correction, and (3) errors in the line flux calibration and measurement. For the S/N of our data, the lowest $E(B-V)$ measurable is 0.01. We therefore assign these 5414 galaxies an upper limit of $E(B-V) < 0.01$.

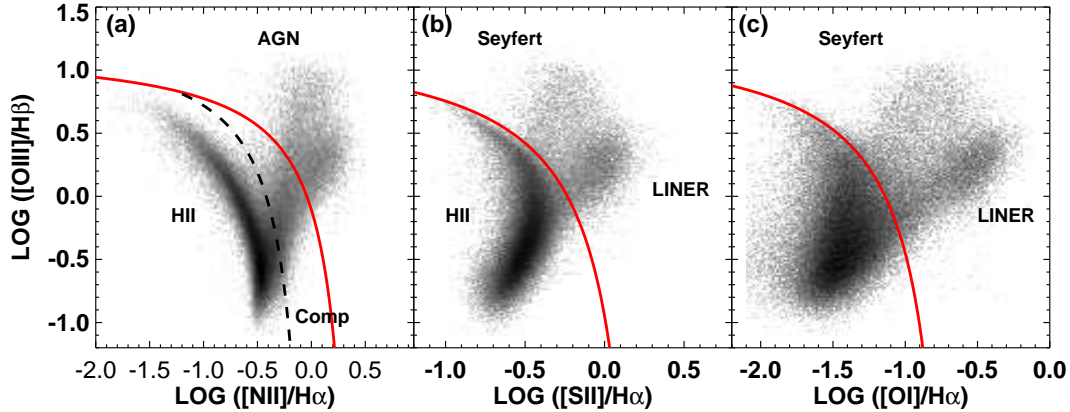


Figure 1. (a) The $[\text{N II}]/\text{H}\alpha$ vs $[\text{O III}]/\text{H}\beta$ diagnostic diagram for SDSS galaxies with $\text{S/N} > 3$. The Kewley et al. (2001a) extreme starburst line and the Kauffmann et al. (2003a) classification line are shown as solid and dashed lines respectively. (b) The $[\text{S II}]/\text{H}\alpha$ vs $[\text{O III}]/\text{H}\beta$ diagnostic diagram, (c) The $[\text{O I}]/\text{H}\alpha$ vs $[\text{O III}]/\text{H}\beta$ diagnostic diagram.

3 OPTICAL CLASSIFICATION

Baldwin et al. (1981) proposed a suite of three diagnostic diagrams to classify the dominant energy source in emission-line galaxies. These diagrams are commonly known as BPT diagrams and are based on the four optical line ratios $[\text{O III}]/\text{H}\beta$, $[\text{N II}]/\text{H}\alpha$, $[\text{S II}]/\text{H}\alpha$, and $[\text{O I}]/\text{H}\alpha$. Kewley et al. (2001a, ; hereafter Ke01) used a combination of stellar population synthesis models and detailed self-consistent photoionization models to create a theoretical “maximum starburst line” on the BPT diagrams. The maximum starburst line is determined by the upper limit of the theoretical pure stellar photoionization models. Galaxies lying above this line are likely to be dominated by an AGN. To rule out possible composite galaxies, Kauffmann et al. (2003a, ; hereafter Ka03) modified the Ke01 scheme to include an empirical line dividing pure star-forming galaxies from Seyfert-H II composite objects whose spectra contain significant contributions from both AGN and star formation.

Figure 1a shows the $[\text{O III}]/\text{H}\beta$ versus $[\text{N II}]/\text{H}\alpha$ standard optical diagnostic diagram for our sample. The Ke01 and Ka03 classification lines are shown as solid and dashed lines. Galaxies that lie below the dashed Ka03 line are classed as H II region-like galaxies. Star-forming galaxies form a tight sequence from low metallicities (low $[\text{N II}]/\text{H}\alpha$, high $[\text{O III}]/\text{H}\beta$) to high metallicities (high $[\text{N II}]/\text{H}\alpha$, low $[\text{O III}]/\text{H}\beta$) which we will refer to as the “star-forming sequence”. The AGN mixing sequence begins at the high metallicity end of the star-forming sequence and extends towards high $[\text{O III}]/\text{H}\beta$ and $[\text{N II}]/\text{H}\alpha$ values. Galaxies that lie in between the two classification lines are on the AGN-H II mixing sequence and are classed as composites. Composite galaxies are likely to contain a metal-rich stellar population plus an AGN. Galaxies that lie above the Ka03 line are classed as AGN.

Figures 1b and 1c show the $[\text{O III}]/\text{H}\beta$ versus $[\text{S II}]/\text{H}\alpha$ and $[\text{O III}]/\text{H}\beta$ versus $[\text{O I}]/\text{H}\alpha$ diagrams for our sample. The Ke01 classification line provides an upper bound to the star-forming sequence on these diagrams. Galaxies that are classed as composites using the $[\text{N II}]/\text{H}\alpha$ diagram (Figure 1a) lie mostly within the star-forming sequence on the $[\text{S II}]/\text{H}\alpha$ diagram (Figure 1b) and about half-way into the

star-forming sequence in the $[\text{O I}]/\text{H}\alpha$ (Figure 1c) diagram. The $[\text{N II}]/\text{H}\alpha$ line ratio is more sensitive to the presence of low-level AGN than $[\text{S II}]/\text{H}\alpha$ or $[\text{O I}]/\text{H}\alpha$ thanks primarily to the metallicity sensitivity of $[\text{N II}]/\text{H}\alpha$. The $\log([\text{N II}]/\text{H}\alpha)$ line ratio is a linear function of the nebular metallicity until high metallicities where the $\log([\text{N II}]/\text{H}\alpha)$ ratio saturates (Kewley & Dopita 2002; Denicoló et al. 2002; Pettini & Pagel 2004). This saturation point causes the star-forming sequence to be almost vertical at $[\text{N II}]/\text{H}\alpha \sim -0.5$. Any AGN contribution shifts the $[\text{N II}]/\text{H}\alpha$ towards higher values than this saturation level, allowing removal of galaxies with even small AGN contributions.

In this work, we classify pure star-forming galaxies as those that lie below the Ka03 line on the $[\text{N II}]/\text{H}\alpha$ vs $[\text{O III}]/\text{H}\beta$ diagnostic diagram. Composite galaxies lie above the Ka03 line and below the Ke01 line. The optical spectra of composites can be due to either (1) a combination of star-formation and a Seyfert nucleus, or (2) a combination of star-formation and LINER emission. The narrow line emission from galaxies lying above the Ke01 line is likely to be dominated by an AGN.

3.1 New LINER, Seyfert, Composite Classification Scheme

It is clear from the $[\text{S II}]/\text{H}\alpha$ and $[\text{O I}]/\text{H}\alpha$ diagrams (Figures 1b and 1c) that galaxies containing AGN lie on two branches. Seyfert galaxies lie on the upper branch while LINERs lie on the lower branch, thanks to their low ionization line emission. We use the $[\text{S II}]/\text{H}\alpha$ and $[\text{O I}]/\text{H}\alpha$ diagrams to separate Seyfert from LINER galaxies. We use only galaxies with $\text{S/N} > 6$ in each of the strong lines to derive our new classification scheme. We define an empirical base point, p (blue circles in Figure 2) and we define annuli with widths of 0.1 dex centered on p . For the galaxies in each of these annuli with radii (R) for which the two AGN branches are well-defined (0.5-1.5 dex from p), we compute histograms of angle from the x-axis. We then step the 0.1 dex annuli through the data from p in 0.02 dex increments and recalculate the minima of each histogram for each increment. A total of 84 histograms were created and minima between

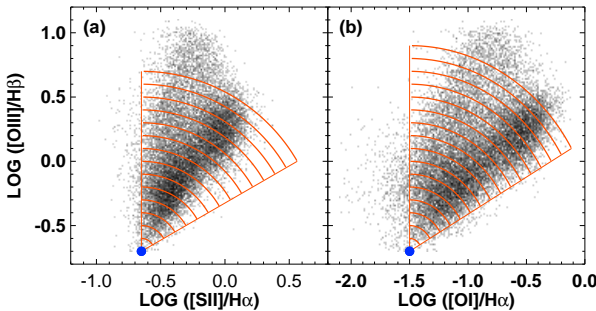


Figure 2. (a) The $[\text{S II}]/\text{H}\alpha$ vs $[\text{O III}]/\text{H}\beta$ and (b) $[\text{O I}]/\text{H}\alpha$ vs $[\text{O III}]/\text{H}\beta$ (right) diagnostic diagrams for SDSS galaxies classified as AGN using the Kauffmann et al. (2003a) line (dashed line in Figure 1a). The large filled circle represents the empirical base point p for the Seyfert and LINER sequences. Concentric arcs of 0.1 dex (red solid lines) show the binning of our sample with radius. We calculate histograms of angle from the x-axis centered at p for each bin.

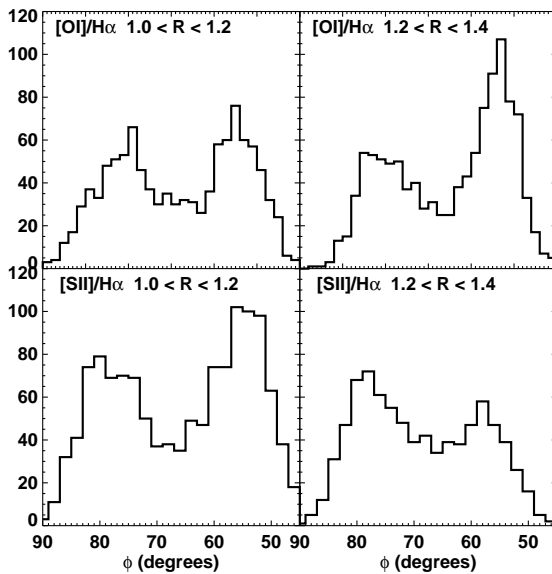


Figure 3. Histograms of the Seyfert and LINER sequences between 1.0-1.2 dex (left) and 1.2-1.4 dex (right) for the $[\text{O I}]/\text{H}\alpha$ (top) and $[\text{S II}]/\text{H}\alpha$ (bottom) diagnostic diagrams. The distribution is clearly bimodal. The LINER sequence is the right-hand peak and the Seyfert sequence is the left-hand peak.

the Seyfert and LINER curves were found for all histograms. Examples of these histograms are given in Figure 3.

To divide between the two AGN branches, we take the line of best-fit through the histogram minima for each of the two diagnostic diagrams. This line provides an empirical division between Seyferts and LINERs and will be referred to as the "Seyfert-LINER classification line". Adding this line to our previous two classification lines from Ke01 and Ka03, we obtain a means to distinguish between star-forming galaxies, Seyferts, LINERs, and composite galaxies. Our new classification scheme is shown in Figure 4, and is defined as follows:

1. **Star-forming galaxies** lie below and to the left of the Ka03 classification line in the $[\text{N II}]/\text{H}\alpha$ vs $[\text{O III}]/\text{H}\beta$ diagram and below and to the left of the Ke01 line in the $[\text{S II}]/\text{H}\alpha$ and $[\text{O I}]/\text{H}\alpha$ diagrams:

$$\log([\text{O III}]/\text{H}\beta) < 0.61/(\log([\text{N II}]/\text{H}\alpha) - 0.5) + 1.3, \quad (1)$$

$$\log([\text{O III}]/\text{H}\beta) < 0.61/(\log([\text{S II}]/\text{H}\alpha) - 0.72) + 0.32, \quad (2)$$

and

$$\log([\text{O III}]/\text{H}\beta) < 0.61/(\log([\text{O I}]/\text{H}\alpha) - 0.73) + 0.59. \quad (3)$$

2. **Composite galaxies** lie between the Ka03 and Ke01 classification lines on the $[\text{N II}]/\text{H}\alpha$ vs $[\text{O III}]/\text{H}\beta$ diagram and below the Ke01 line on the $[\text{S II}]/\text{H}\alpha$ and $[\text{O I}]/\text{H}\alpha$ diagrams:

$$0.61/(\log([\text{N II}]/\text{H}\alpha) - 0.5) + 1.3 < \log([\text{O III}]/\text{H}\beta), \quad (4)$$

$$\log([\text{O III}]/\text{H}\beta) < 0.61/(\log([\text{N II}]/\text{H}\alpha) - 0.47) + 1.19, \quad (5)$$

$$\log([\text{O III}]/\text{H}\beta) < 0.61/(\log([\text{S II}]/\text{H}\alpha) - 0.72) + 0.32, \quad (6)$$

and

$$\log([\text{O III}]/\text{H}\beta) < 0.61/(\log([\text{O I}]/\text{H}\alpha) - 0.73) + 0.59. \quad (7)$$

3. **Seyfert galaxies** lie above the Ke01 classification line on the $[\text{N II}]/\text{H}\alpha$, $[\text{S II}]/\text{H}\alpha$, and $[\text{O I}]/\text{H}\alpha$ diagnostic diagrams and above the Seyfert-LINER line on the $[\text{S II}]/\text{H}\alpha$ and $[\text{O I}]/\text{H}\alpha$ diagrams, i.e.

$$0.61/(\log([\text{N II}]/\text{H}\alpha) - 0.47) + 1.19 < \log([\text{O III}]/\text{H}\beta), \quad (8)$$

$$0.61/(\log([\text{S II}]/\text{H}\alpha) - 0.72) + 0.32 < \log([\text{O III}]/\text{H}\beta), \quad (9)$$

$$0.61/(\log([\text{O I}]/\text{H}\alpha) - 0.73) + 0.59 < \log([\text{O III}]/\text{H}\beta), \quad (10)$$

and

$$0.76 \log([\text{S II}]/\text{H}\alpha + 1.89) < \log([\text{O III}]/\text{H}\beta), \quad (11)$$

$$1.30 \log([\text{O I}]/\text{H}\alpha + 1.18) < \log([\text{O III}]/\text{H}\beta). \quad (12)$$

4. **LINERs** lie above the Ke01 classification line on the $[\text{N II}]/\text{H}\alpha$, $[\text{S II}]/\text{H}\alpha$, and $[\text{O I}]/\text{H}\alpha$ diagnostic diagrams and below the Seyfert-LINERs line on the $[\text{S II}]/\text{H}\alpha$ and $[\text{O I}]/\text{H}\alpha$ diagrams, i.e.

$$0.61/(\log([\text{N II}]/\text{H}\alpha) - 0.47) + 1.19 < \log([\text{O III}]/\text{H}\beta), \quad (13)$$

$$0.61/(\log([\text{S II}]/\text{H}\alpha) - 0.72) + 0.32 < \log([\text{O III}]/\text{H}\beta), \quad (14)$$

$$\log([\text{O III}]/\text{H}\beta) < 0.76 \log([\text{S II}]/\text{H}\alpha + 1.89), \quad (15)$$

$$0.61/(\log([\text{O I}]/\text{H}\alpha) - 0.73) + 0.59 < \log([\text{O III}]/\text{H}\beta) \quad (16)$$

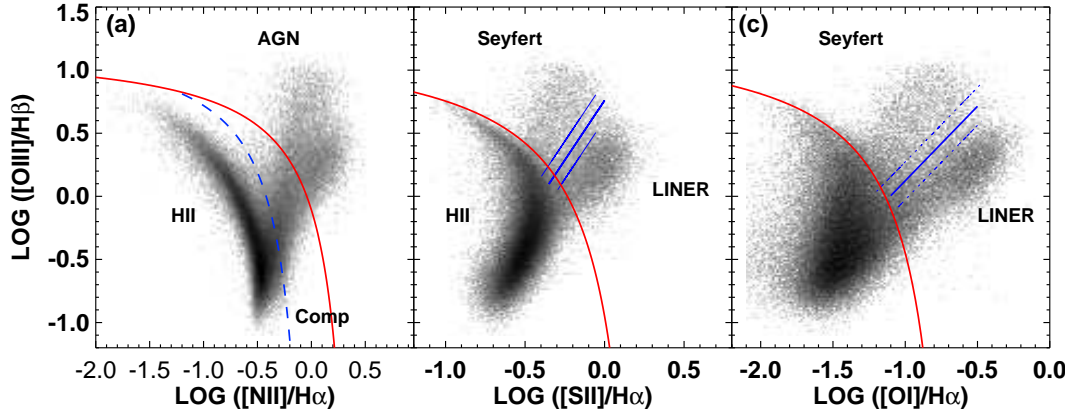


Figure 4. The three BPT diagrams showing our new scheme for classifying galaxies using emission-line ratios. The Kewley et al. (2001a) extreme starburst classification line (red solid), the Kauffmann et al. (2003a) pure star-formation line (blue dashed), and our new Seyfert-LINER line (blue solid) are used to separate galaxies into H II region-like, Seyferts, LINERs, and Composite H II-AGN types.

$$\log([OIII]/H\beta) < 1.30 \log([OI]/H\alpha) + 1.18, \quad (17)$$

5. **Ambiguous galaxies** are those that are classified as one type of object in one or or two diagrams and classified as another type of object in the remaining diagram(s). In our scheme, ambiguous galaxies fall into one of two categories: (a) galaxies that lie in the Seyfert region in either the [S II]/H α or [O I]/H α diagram and in the LINER region in the remaining ([O I]/H α or [S II]/H α) diagram, or (b) galaxies that lie in the composite region (below the Ke01 line) in the [N II]/H α diagram but that lie above the Ke01 line in either the [S II]/H α or [O I]/H α diagram.

According to this scheme, our 85224-galaxy sample contains 63893 (75%) star-forming galaxies, 2411 (3%) Seyferts, 6005 (7%) LINERs, and 5870 (7%) composites. The remaining galaxies are ambiguous galaxies (7045; 8%).

3.1.1 Simple Diagnostic Diagram

Using the classifications obtained in the previous section, we investigate other line diagnostic diagrams that may be able to separate the different classes in a simpler way. Figure 5 shows the [O III]/[O II] vs [O I]/H α diagnostic diagram for the H II-region like Seyferts, LINERs, and composites. We exclude ambiguous objects from this plot. LINERs and Seyferts form two distinct groups on this diagram and both groups are easily separated from the H II region-like galaxies and composites. The reason for this clean separation is twofold; [O III]/[O II] is a sensitive diagnostic of the ionization parameter of the gas, while [O I]/H α is sensitive to the hardness of the ionizing radiation field. The ionization parameter is a measure of the amount of ionization that a radiation field can drive as it moves through the nebula. Seyfert galaxies have a higher ionization parameter than LINERs (by definition) or star-forming galaxies and therefore Seyferts separate vertically ([O III]/[O II]) from the other classes of objects. Both Seyfert galaxies and LINERs have hard power-law ionizing radiation fields and thus separate from star-forming galaxies in the horizontal ([O I]/H α) di-

rection. Interestingly, composite galaxies lie within the star-forming sequence on this diagram, indicating that the hardness of the ionizing radiation field, and the ionization parameter of composites are likely to be dominated by their star-formation.

To calculate an empirical separation between LINERs, Seyferts, and H II+composites, we find the minima of a 2-dimensional histogram of [O III]/[O II] and [O I]/H α . These minima are fit with a least-squares line of best-fit. The resulting empirical separations are shown in blue. For comparison, the Heckman (1980) classification line is shown (purple dashed line). Clearly the Heckman classification scheme would separate most LINERs from Seyfert galaxies. This diagnostic diagram is a more simple method for separating LINERs, Seyferts, and star-forming galaxies (including composites). Our separations are given by;

H II & Composites:

$$\log([OIII]/[OII]) < -1.701 \log([OI]/H\alpha) - 2.163 \quad (18)$$

LINERs:

$$-1.701 \log([OI]/H\alpha) - 2.163 < \log([OIII]/[OII]) \quad (19)$$

$$\log([OIII]/[OII]) < 1.0 \log([OI]/H\alpha) + 0.7 \quad (20)$$

Seyferts:

$$-1.701 \log([OI]/H\alpha) - 2.163 < \log([OIII]/[OII]) \quad (21)$$

$$1.0 \log([OI]/H\alpha) + 0.7 < \log([OIII]/[OII]) \quad (22)$$

Note that the [O III]/[O II] vs [O I]/H α diagram should not be used to separate H II galaxies from composite objects and it relies on accurate reddening correction between [O III] $\lambda 5007$ and [O II] $\lambda 3727, 29$.

3.1.2 Comparison with Previous Diagnostic Schemes

In Figure 6 we compare our new classification scheme with previous methods of classification. The solid green line shows

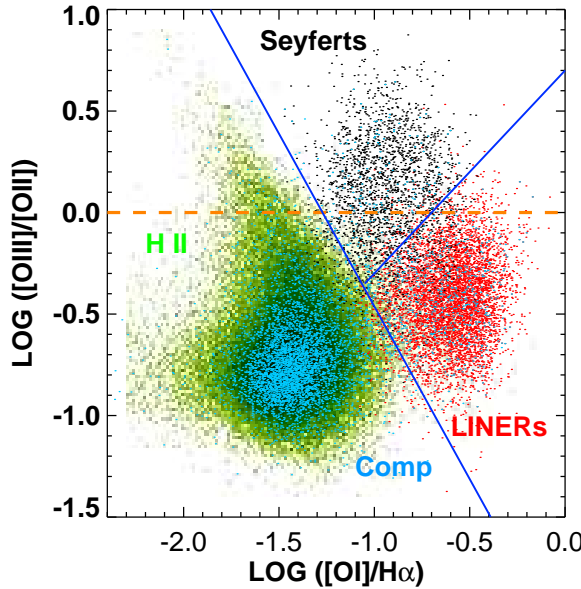


Figure 5. The $[\text{O III}]/[\text{O II}]$ vs $[\text{O I}]/\text{H}\alpha$ diagnostic diagram for SDSS galaxies with $S/N > 3$. Galaxies have been classified using the standard BPT diagnostic diagrams (Figure 4). Ambiguous galaxies are not included. Our new preferred classification scheme is shown in blue. The Heckman (1980) LINER line (purple dashed) is also shown.

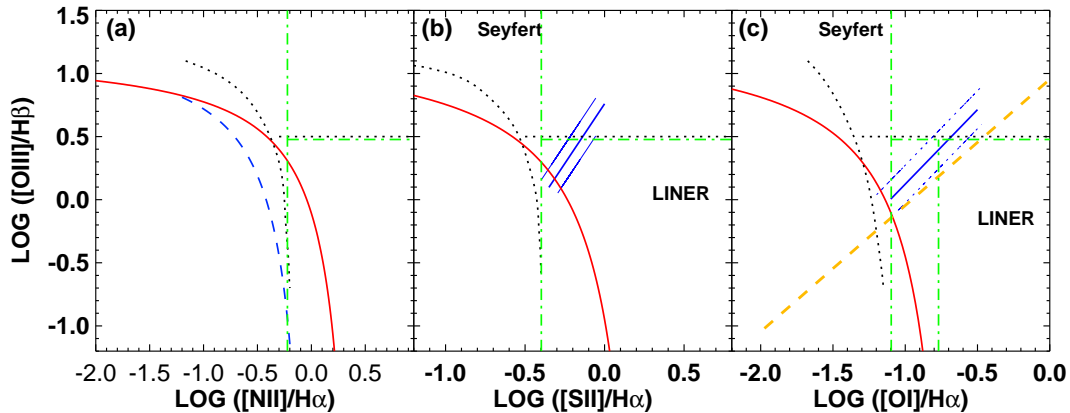


Figure 6. The three BPT diagrams showing different methods for classifying galaxies using emission-line ratios. The Kewley et al. (2001a) extreme starburst classification line (red solid), the Kauffmann et al. (2003a) pure star-formation line (blue dashed), our new Seyfert-LINER line (blue solid), the Veilleux & Osterbrock (1987) classification scheme (black dotted), the Heckman (1980) LINER line (purple dashed), and the Ho et al. (1997) classification schemes (green dot-dashed) are shown.

where the Heckman (1980, ; hereafter H80) LINER classification line lies in relation to our Seyfert-LINER line. H80 defined LINERs as having $[\text{O II}] \lambda 3727 \gtrsim [\text{O III}] \lambda 5007$ and $[\text{O I}] \lambda 6300 \lambda 6300 \gtrsim 1/3 [\text{O III}] \lambda 5007$. The H80 line has a very similar slope to our Seyfert-LINER line and is close to the 0.1 dex error markers for our line. The H80 LINER criteria are sometimes used in combination with additional line ratio criteria using $[\text{O III}]/\text{H}\beta$ and/or $[\text{N II}]/\text{H}\alpha$, $[\text{S II}]/\text{H}\alpha$, $[\text{O I}]/\text{H}\alpha$ to remove star-forming galaxies (e.g., Heckman et al. 1983). Using our "extreme starburst line" to remove galaxies dominated by their star formation (including composites), we find that all galaxies that are classed

as LINERs using the H80 criteria are also classed as LINERs using our scheme. Conversely, approximately 56% of our LINERs are also classified as LINERs using the H80 scheme. The remaining galaxies lie above the H80 line but below our Seyfert-LINER dividing line. If we do not remove star-forming galaxies and we impose the H80 criteria ($[\text{O II}] \lambda 3727 \gtrsim [\text{O III}] \lambda 5007$ and $[\text{O I}] \lambda 6300 \lambda 6300 \gtrsim 1/3 [\text{O III}] \lambda 5007$), then 15% of galaxies that are classed as LINERs using the H80 criteria are also classed as LINERs in our scheme. The remaining 85% are H II galaxies (68%), composites (7%), and ambiguous galaxies (9%). Al-

ternatively, $\sim 78\%$ of our LINERs are also classed as LINERs using the H80 scheme.

An alternative classification scheme was proposed by VO87 for galaxies where $[\text{O II}]$ is not measured. The VO87 scheme is shown in Figure 6 (black dotted lines). If our classification is correct, galaxies classified as LINERs according to the VO87 scheme are either true LINERs, Seyferts, or composites. Of the galaxies classified as LINERs in the VO87 scheme, 67% are LINERs, 5% are Seyferts, 4% are composites, 0.01% are H II region-like, and 23% are ambiguous objects. These ambiguous objects are likely to be composites or transition objects because they lie within the composite region in one or two of the BPT diagrams and in the AGN region in the remaining diagrams. On the other hand, approximately 87% of our LINERs are also classified as LINERs using the VO87 method.

(Ho et al. 1997, ; hereafter HFS97) defined a new classification scheme for the four different classes of objects using the nuclear emission-line ratios of 418 galaxies. Their classification scheme is shown on Figure 6 as green dot-dashed lines. The HFS97 LINERs criterion for $[\text{O I}]/\text{H}\alpha$ and $[\text{O III}]/\text{H}\beta$ begins on our Seyfert-LINER classification line. Because of this LINER criterion, 92% of galaxies classed as LINERs in the HFS97 scheme are also LINERs in our scheme. The remaining 8% are ambiguous objects that lie within our LINER region on one or more diagrams and within the Seyfert region on the remaining diagrams.

To conclude, because $\sim 90\text{--}100\%$ of galaxies classified using H80 (with reliable removal of H II galaxies) or HFS97 as LINERs remain LINERs in our scheme, previous studies of LINERs defined according to H80 or HFS97 should reflect the true properties of LINERs. In contrast, $\sim 1/3$ of objects in LINER studies that have used the VO87 scheme may be AGN-H II composites and Seyferts. Without pre-removal of H II galaxies, the H80 scheme includes a substantial fraction (68%) of H II galaxies. The relative ratio of composite, Seyfert, and true LINERs will depend on any additional selection criteria used in previous LINERs surveys (such as luminosity or color selection).

3.1.3 Completeness and Aperture effects as a Function of Class

At redshifts $z < 0.01$ we can detect galaxies with $M_* > 10^{10} M_\odot$ irrespective of their stellar mass-to-light ratios. Thus we only consider galaxies with masses greater than $10^{10} M_\odot$ in this analysis. We note that the fraction of galaxies with masses less than $10^{10} M_\odot$ is small (4%).

In Figure 7, we show how the fraction of non-H II galaxies classed as Seyfert, LINER and composite changes over the redshift range of our sample. Ambiguous galaxies are not shown. The fraction of LINERs falls with redshift from $z \sim 0.045$ to $z \sim 0.1$ in the $11 < \log(M) < 11.5$ mass range, $z \sim 0.03$ to $z \sim 0.1$ in the $10.5 < \log(M) < 11$ mass range, and $z \sim 0.1$ to $z \sim 0.1$ in the $10 < \log(M) < 10.5$ mass range. This drop in LINER fraction is similar to the slope that Kauffmann et al. (2003a) found for low luminosity AGN ($\log(L[\text{OIII}]) < 7 L_\odot$). The drop occurs because weak emission lines become increasingly difficult to detect as the physical aperture subtended by the SDSS fibre becomes larger. Over the redshift range $0.04 < z < 0.1$, the

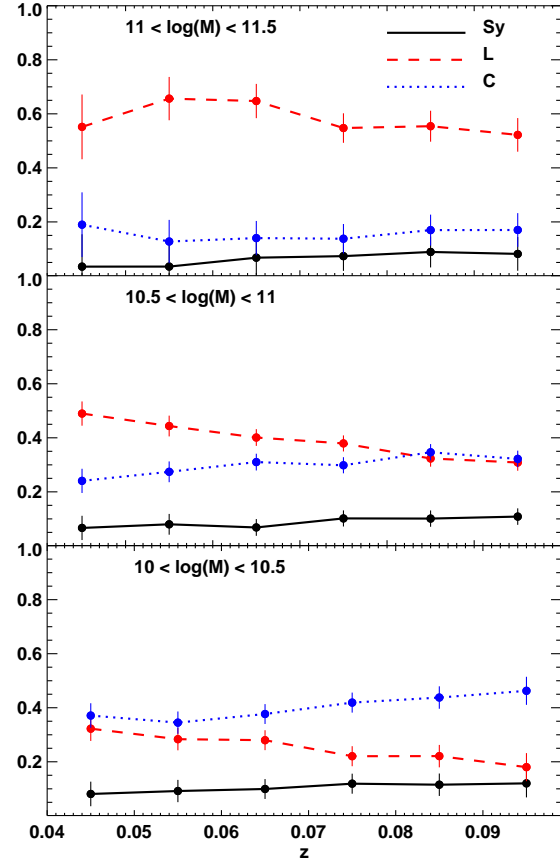


Figure 7. The fraction of galaxies classified as Seyfert (black solid), LINER (red dashed), and composite (blue dotted) as a function of redshift within three mass ranges. Ambiguous galaxies are not included in this plot.

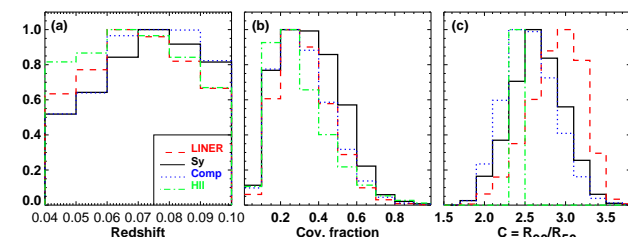


Figure 8. The distribution of (a) redshift, (b) g-band fiber covering fraction, and (c) concentration for non-H II galaxies classified as Seyfert (black solid line), LINER (red dashed line), and composite (blue dotted line) as a function of redshift within for mass ranges. Ambiguous galaxies are not included in this plot.

change in LINER fraction is not very large, so aperture bias should not affect our conclusions substantially.

Figure 8 shows the overall redshift distribution, g-band fiber covering fraction, and concentration index of each spectral type.

LINERs have redshift distributions skewed towards lower redshifts than Seyferts or composites, as already seen

in Figure 7. Figure 8c indicates that the LINERs in our sample are more concentrated than Seyferts or composites. LINERs have only a slightly lower mean g-band fiber covering fraction for LINERs (0.34 ± 0.01) than for Seyfert galaxies (0.36 ± 0.01) Figure 8b). Because the difference in g-band covering fraction between Seyferts and LINERs is small, we proceed with our analysis of the host properties of LINERs and Seyferts.

4 STAR-FORMING DISTANCE

To explore the host properties as a function of distance from the star-forming sequence, we define an empirical linear distance (in dex) from the star-forming sequence for both the Seyfert and LINER branches on the $[\text{O III}]/\text{H}\beta$ vs $[\text{O I}]/\text{H}\alpha$ diagnostic diagram shown in Figure 9. A base point (red and blue circles in Figure 9) is defined for each branch. A peak radius of 1.55 dex from the base point is defined for Seyferts. The peak radius is 1.65 dex for LINERs. The distance between the peak radius and the base point for each branch is divided into ten bins. The position of the base and peak points have been chosen to ensure that the first and last bins contain at least 50 data points.

Note that because D_{SF} is defined in dex in log line-ratio space, it does not give the fraction of star-formation or AGN emission in a galaxy.

In Figure 10 we show the relative ratio of Seyferts and LINERs as a function of D_{SF} . In this plot, we include composite Seyfert+H_{II} and LINER+H_{II} (classified using our Seyfert-LINER dividing line) as Seyferts and LINERs respectively. Only pure star-forming galaxies classified according to the Ka03 classification line (equation 1) and LINER/Seyfert ambiguous galaxies are excluded from Figure 10. The composite-pure AGN boundary corresponds roughly to $D_{SF} = 0.3 - 0.4$.

Figure 10 shows that the ratio of Seyfert to LINERs remains roughly constant with distance from the star-forming sequence. This result is unexpected because both Seyfert-H_{II} and LINER-composites exist and there is a large luminosity difference between Seyferts and LINERs. One might expect that in Seyfert-H_{II} composites, the stellar emission would be overwhelmed by the luminous Seyfert emission while in LINERs, stellar emission could dominate in many LINER-H_{II} composites. If this expectation were correct, there should be many more LINER-H_{II} composites than Seyfert-H_{II} composites. The fact that the Seyfert to LINER ratio is roughly independent of d_{SF} (Figure 10) implies that star formation and AGN are coupled such that more powerful AGN also have stronger star formation.

5 HOST PROPERTIES

Using our new classification scheme, we explore the host properties of the AGN in our sample. The host properties of AGN in the SDSS were previously studied by Kauffmann et al. (2003a). They used the $[\text{O III}]$ luminosity to discriminate between Seyferts and low-luminosity AGN. The following analysis extends this work by comparing the host properties of LINERs, Seyferts and composites as a function of distance from the star-forming sequence.

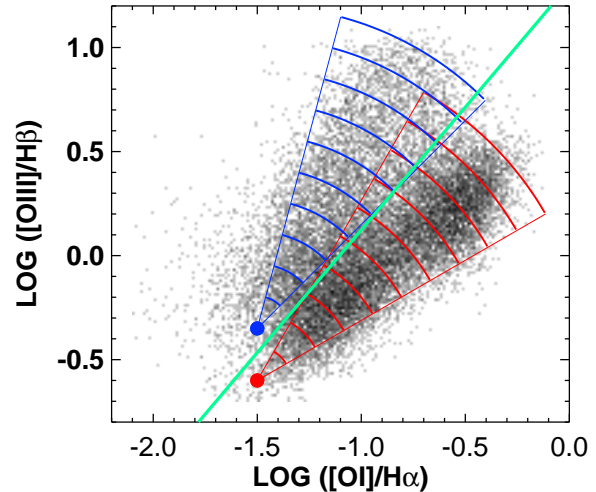


Figure 9. The $[\text{O III}]/\text{H}\beta$ vs $[\text{O I}]/\text{H}\alpha$ diagnostic diagram for the AGN in the SDSS sample. Colored curves correspond to our empirical definition of distance from the star-forming sequence D_{SF} . Blue and red curves give lines of constant D_{SF} for Seyferts and LINERs respectively. The green line shows the dividing line between Seyferts and LINERs.

5.1 Stellar Population Age

We use the 4000Å break ($D4000$) and the H δ Balmer absorption line as indicators of the age of the stellar population. The 4000Å break is created by absorption lines located around 4000Å and was first defined by Bruzual A. (1983), and recently redefined by Balogh et al. (1999) as:

$$D4000 = \frac{\int_{4000}^{4100} f_\lambda d\lambda}{\int_{3850}^{3950} f_\lambda d\lambda} \quad (23)$$

The strength of the 4000Å break is influenced by temperature and metallicity. As the temperature of the stellar atmospheres decreases with age, the metal opacity strengthens and $D4000$ becomes large. $D4000$ was calibrated empirically by Gorgas et al. (1999) and theoretically by Bruzual & Charlot (2003). The theoretical calibrations predict that $D4000$ provides a reliable estimate of the galaxy age for galaxies with mean stellar ages less than a few Gyr. In the presence of current or recent star formation, $D4000$ is small because the metal opacity in the atmospheres of O and B stars weakens.

A complementary age indicator is the equivalent width (EW) of the H δ absorption line. The H δ absorption line is produced in the atmospheres of A to G stars and is useful for predicting the age of bursts that ended 4Myr - 1 Gyr ago (González Delgado et al. 1999; Worthey & Ottaviani 1997). We use the $H\delta_A$ index defined by Worthey & Ottaviani (1997):

$$H\delta_A = (4091.00 - 4112.25)/(1 - F_I/F_C) \quad (24)$$

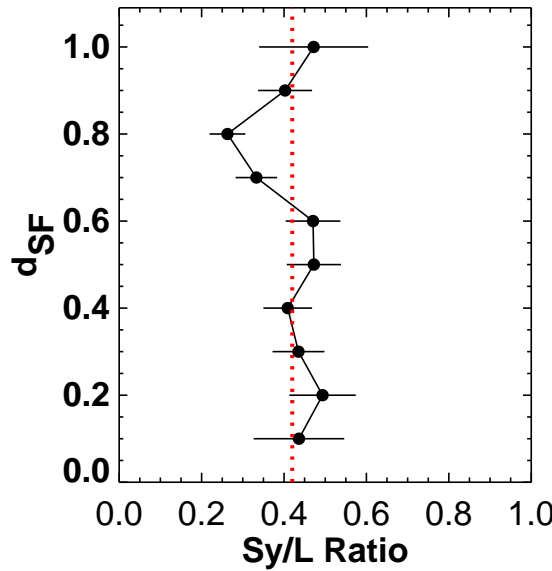


Figure 10. The ratio of Seyferts to LINERs as a function of D_{SF} . The dotted line shows the mean Seyfert to LINER ratio.

where F_I is the flux within the (4091.00 - 4112.25) bandpass and F_C is the pseudo-continuum flux within the bandpass.

The evolution of D_{4000} and $H\delta_A$ have been investigated by Kauffmann et al. (2003c) using high resolution spectral libraries and the Bruzual & Charlot (2003) stellar population synthesis models. They find that neither index depends strongly on metallicity until at least 1 Gyr after the burst.

In Figure 11a, we show the normalized distribution of D_{4000} for LINERs (red). For comparison, we plot the D_{4000} distributions for Seyferts (black), composites (blue), and H II region-like galaxies (green). The stellar population of LINERs is older than the other galaxy types. Seyferts and composites have a similar range of stellar ages, and H II region-like galaxies are dominated by relatively young star-forming regions, as expected.

To avoid biasing our analysis against galaxies that contain significant star formation, in Figure 11b we give the normalized distribution of D_{4000} without defining composites as a separate class. Rather, we use our Seyfert-LINER classification line to divide the composite galaxies into H II+LINER and H II+Seyfert classes. We include H II+LINER and H II+Seyfert in the LINER and Seyfert classes respectively. Only pure star-forming galaxies classified according to the Ka03 classification line (equation 1) and LINER/Seyfert ambiguous galaxies are excluded. Comparison of panels (a) and (b) shows that while the difference between Seyferts and LINERs is somewhat reduced if the composites are included, there is still a very clear age offset between the two classes.

In Figure 11c, we show how the stellar population evolves as a function of D_{SF} for Seyferts, composites, LINERs, and ambiguous galaxies. Figure 11d gives the median D_{4000} at each 0.1 interval of D_{SF} . Composites are included in the LINER and Seyfert classes as in Figure 11b. Pure LINERs and Seyferts correspond roughly to a D_{SF} of 0.5.

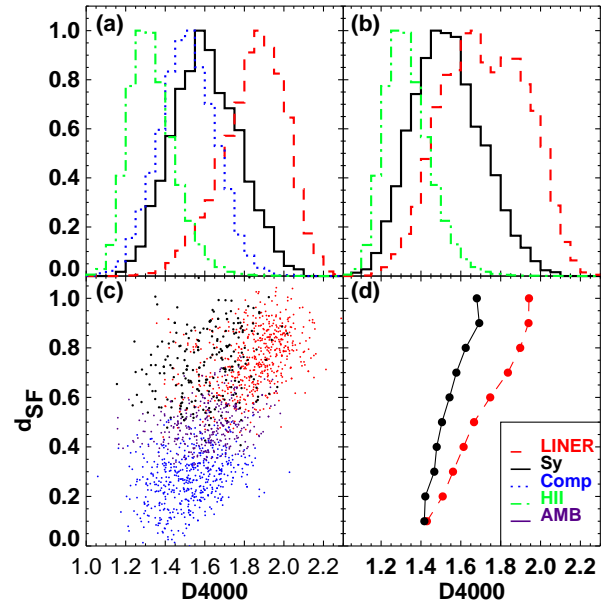


Figure 11. (a) The distribution of D_{4000} for LINERs (red dashed), Seyferts (black solid), composites (blue dotted) and H II region-like galaxies (green dot-dashed). (b) The distribution of D_{4000} for LINERs (red-dashed), Seyferts (black solid), and H II region-like galaxies (green dot-dashed) where LINERs and Seyferts include LINER+H II and Seyfert+H II composites. Only pure star-forming galaxies classified according to the Ka03 classification line (equation 1) and LINER/Seyfert ambiguous galaxies are excluded. (c) D_{4000} for a uniform random sampling of the Seyferts (black) and LINERs (red), composites (blue) and ambiguous galaxies (purple) as a function of distance from the Ke01 line. (d) The median D_{4000} for Seyferts (black) and LINERs (red) as a function of distance from the Ke01 line, including Seyfert+H II and LINER+H II galaxies. A distance of 1.0 indicates that the optical line ratios are dominated by ionizing radiation from the Seyfert or LINER nucleus.

The correlation coefficients and corresponding significance of the correlation are given in Table 1. Clearly D_{SF} and D_{4000} are strongly correlated for both LINERs and Seyferts. Both types of objects have young stellar populations typical of active star-forming galaxies at low D_{SF} , by definition. Both Seyfert and LINER hosts have older stellar populations at large D_{SF} . LINER hosts have an older stellar population than Seyferts at all but the smallest D_{SF} . Figure 12 shows that a similar trend holds for $H\delta_A$.

5.2 Stellar Mass

The SDSS stellar masses were derived by Kauffmann et al. (2003b), and Gallazzi et al. (2005) using a combination of z -band luminosities and Monte Carlo stellar population synthesis fits to D_{4000} and $H\delta$. The model fits provide powerful constraints on the star formation history and metallicity of each galaxy, thus providing a more reliable indicator of mass than assuming a simple mass-to-light ratio. Drory et al. (2005) compared $\sim 17,000$ SDSS spectroscopically derived masses with (a) masses derived from population synthesis fits to the broadband SDSS and 2MASS colors, and (b) masses calculated from SDSS velocity dis-

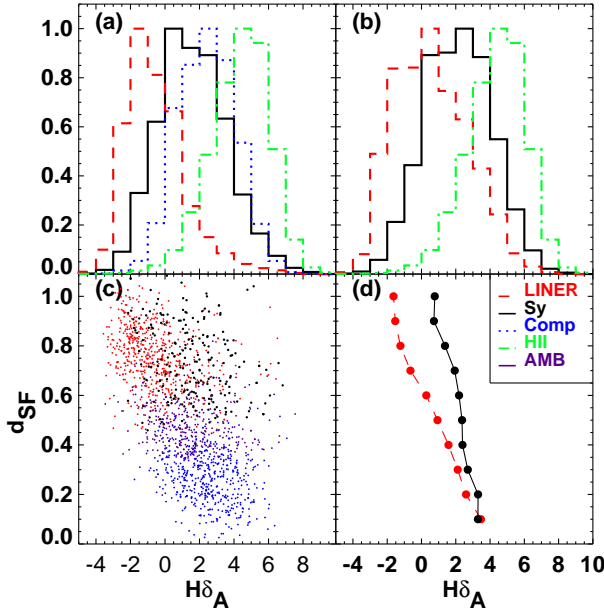


Figure 12. (a) The distribution of $H\delta_A$ for LINERs (red dashed), Seyferts (black solid), composites (blue dotted) and H II region-like galaxies (green dot-dashed). (b) The distribution of $H\delta_A$ for LINERs (red-dashed), Seyferts (black solid), and H II region-like galaxies (green dot-dashed) where LINERs and Seyferts include LINER+H II and Seyfert+H II composites. (c) $H\delta_A$ for a uniform random sampling of the Seyferts (black) and LINERs (red), composites (blue) and ambiguous galaxies (purple) as a function of distance from the Ke01 line. (d) The median $H\delta_A$ for Seyferts (black) and LINERs (red) as a function of distance from the Ke01 line, including Seyfert+H II and LINER+H II galaxies. A distance of 1.0 indicates that the optical line ratios are dominated by ionizing radiation from the Seyfert or LINER nucleus.

persions and effective radii. They concluded that the three methods for estimating mass agree to within ~ 0.2 dex over the $10^8 - 10^{12} M_\odot$ range.

The stellar mass distribution of SDSS emission-line galaxies was studied previously by Kauffmann et al. (2003a). They find a strong dependence between the fraction of galaxies containing AGN and stellar mass. Figure 13a confirms this result. The stellar mass distribution of star-forming galaxies (green dot-dashed line) is shifted substantially towards lower masses compared to the mass distributions of composites, Seyferts, or LINERs. Figure 13a shows that the stellar mass of LINER galaxies is slightly higher than for Seyfert galaxies. Composite objects have a very similar mass distribution to Seyfert galaxies but this may be a coincidence; only a small fraction (14%) of composites lie above the Seyfert-LINER dividing line on both $[\text{N II}]/\text{H}\alpha$ and $[\text{S II}]/\text{H}\alpha$ diagrams. The majority of composites (67%) lie on the H II-LINER sequence and therefore these galaxies may simply have stellar masses intermediate between H II region-like galaxies and LINERs. The median stellar mass of the composite galaxies ($\log(M_*) = 10.54$) is within 0.02 dex of the average of the median stellar mass for H II region-like and LINER classes (10.52).

Figure 13d shows that the stellar mass is roughly constant as a function of D_{SF} . There is only a small correlation

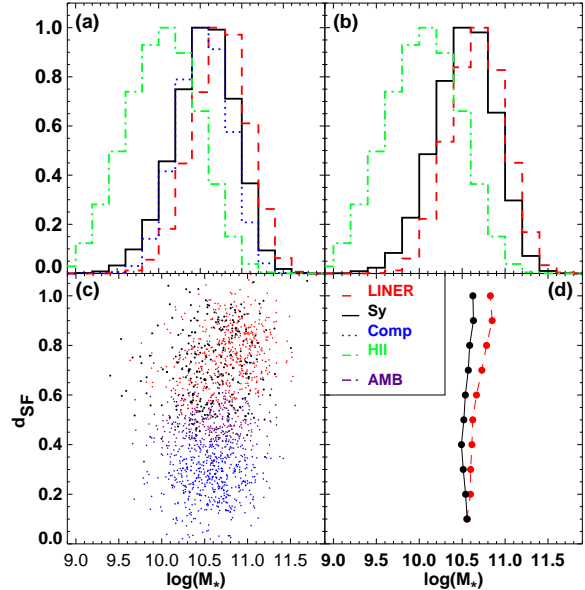


Figure 13. (a) The distribution of the logarithm of the stellar mass (M_*) for LINERs (red dashed), Seyferts (black solid), composites (blue dotted) and H II region-like galaxies (green dot-dashed). (b) The distribution of M_* for LINERs (red-dashed), Seyferts (black solid), and H II region-like galaxies (green dot-dashed) where LINERs and Seyferts include LINER+H II and Seyfert+H II composites. (c) M_* for a uniform random sampling of the Seyferts (black) and LINERs (red), composites (blue) and ambiguous galaxies (purple) as a function of distance from the Ke01 line. (d) The median M_* for Seyferts (black) and LINERs (red) as a function of distance from the Ke01 line, including Seyfert+H II and LINER+H II galaxies. A distance of 1.0 indicates that the optical line ratios are dominated by ionizing radiation from the Seyfert or LINER nucleus.

between SF distance and stellar mass for Seyferts and a stronger correlation for LINERs (Table 1).

5.3 Mass-to-Light Ratio

To investigate how the mass of galaxies at a given observed luminosity changes between the different spectral types, we use the median z-band mass-to-light (M/L) ratios. The M/L ratio of galaxies is influenced by the age of the stellar population and the attenuation by dust.

The SDSS M/L ratios were derived by Kauffmann et al. (2003b) using Monte Carlo simulations of different star formation histories. They find that the M/L ratio correlates strongly with galaxy luminosity such that luminous galaxies have high M/L ratios while faint galaxies have a wide range of M/L ratios. Kauffmann et al. (2003b) used stellar evolution models to predict how M/L changes as a function of galaxy luminosity, and stellar population age. They show that the majority of luminous galaxies have M/L ratios consistent with having formed stars at constant rate over a Hubble time, and that faint galaxies have formed most of their stars closer to the present. This effect is reflected in Figure 14a where we plot the normalized distribution of M/L for star-forming galaxies, LINERs, Seyferts and Composites. Seyferts, LINERs and composites have similar M/L

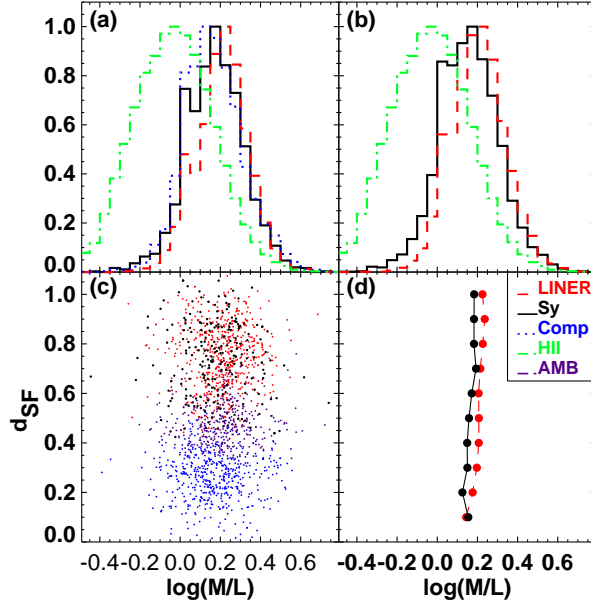


Figure 14. (a) The distribution of the logarithm of the stellar mass-to-light ratio (M/L) for LINERs (red dashed), Seyferts (black solid), composites (blue dotted) and H II region-like galaxies (green dot-dashed). (b) The distribution of M/L for LINERs (red-dashed), Seyferts (black solid), and H II region-like galaxies (green dot-dashed) where LINERs and Seyferts include LINER+H II and Seyfert+H II composites. (c) M/L for a uniform random sampling of the Seyferts (black) and LINERs (red), composites (blue) and ambiguous galaxies (purple) as a function of distance from the Ke01 line. (d) The median M/L for Seyferts (black) and LINERs (red) as a function of distance from the Ke01 line, including Seyfert+H II and LINER+H II galaxies. A distance of 1.0 indicates that the optical line ratios are dominated by ionizing radiation from the Seyfert or LINER nucleus.

distributions, with LINERs having only slightly larger M/L ratios on average than Seyferts or composites. The median M/L ratio is 0.21 dex for LINERs, 0.18 dex for Seyferts and 0.16 dex for composites (the standard error of the median is small; 0.002–0.004 dex). The M/L range of H II region-like galaxies is substantially lower than for the other galaxy types, including composites. The M/L range of H II region-like galaxies is consistent with their having had present star formation and substantial dust as expected. In H II region-like galaxies, the M/L ratio is correlated with metallicity. The relatively high M/L ratio of composites may therefore result from their metal-rich stellar population. The M/L ratio does not change as a function of D_{SF} (Figure 14d).

5.4 Stellar Velocity Dispersion

The stellar velocity dispersion σ_* in a galaxy containing an AGN is related to the black hole mass (Tremaine et al. 2002). Figure 15a shows the σ_* distribution for each of the galaxy types and the relationship between σ_* and D_{SF} . LINERs have a broader distribution of σ_* than Seyferts or composites. When composite LINER+H II and Seyfert+H II galaxies are included in the LINER and Seyfert classes (Figure 15b), it is clear that the σ_* distribution for LINERs has a larger tail towards high σ_* values.

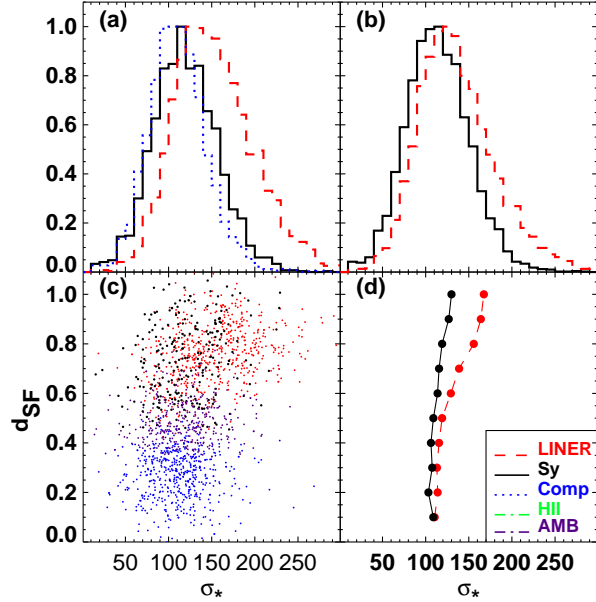


Figure 15. (a) The distribution of the logarithm of the stellar velocity dispersion (σ_*) for LINERs (red dashed), Seyferts (black solid), composites (blue dotted) and H II region-like galaxies (green dot-dashed). (b) The distribution of σ_* for LINERs (red-dashed), Seyferts (black solid), and H II region-like galaxies (green dot-dashed) where LINERs and Seyferts include LINER+H II and Seyfert+H II composites. (c) σ_* for a uniform random sampling of the Seyferts (black) and LINERs (red), composites (blue) and ambiguous galaxies (purple) as a function of distance from the Ke01 line. (d) The median σ_* for Seyferts (black) and LINERs (red) as a function of distance from the Ke01 line, including Seyfert+H II and LINER+H II galaxies. A distance of 1.0 indicates that the optical line ratios are dominated by ionizing radiation from the Seyfert or LINER nucleus.

Figure 15d also shows that σ_* is roughly constant with D_{SF} for Seyfert galaxies, with only a slight increase in σ_* (~ 20 km/s), indicating that black hole mass is relatively constant along the Seyfert branch but that black hole mass may be somewhat larger at high D_{SF} . We show that σ_* is strongly correlated with the optical line ratios, or D_{SF} for pure LINERs.

5.5 [OIII] Luminosity

In Figure 16a we show the extinction-corrected [O III] luminosity distribution for each spectral class. LINERs have a lower median [O III] luminosity than any of the other spectral types; $med(\log L([OIII])) = 6.1 L_\odot$ for LINERs and $med(\log L([OIII])) = 6.3, 6.5, \text{ and } 7.3 L_\odot$ for H II region-like, composites and Seyferts respectively. Seyferts have substantially larger $L[OIII]$ than the other spectral classes from the hard ionizing continuum produced by their AGN. Composite galaxies have a slightly higher median $L[OIII]$ than H II region-like galaxies and substantially higher median $L[OIII]$ than LINERs. As discussed in Section 5.2, the majority of composites lie on the LINER branch, but 15% lie on the Seyfert branch. The large $L[OIII]$ luminosity of these Seyferts raises the median $L[OIII]$ for composites.

The median [O III] luminosity rises as a function of

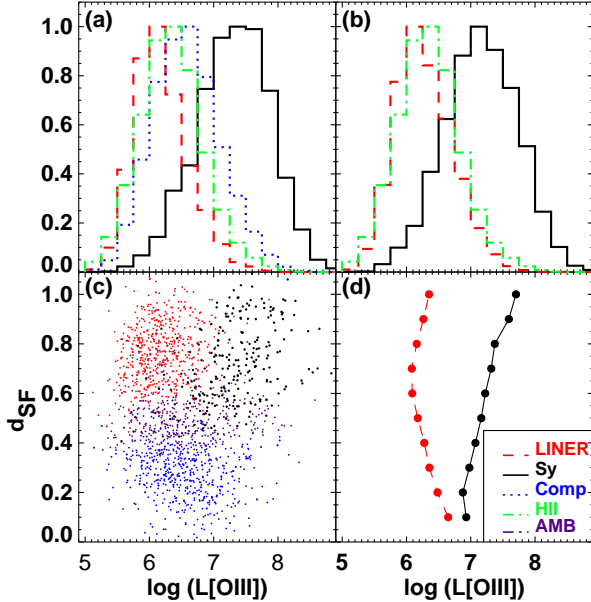


Figure 16. (a) The distribution of the logarithm of the extinction-corrected [OIII] luminosity (L_{\odot}) for LINERs (red dashed), Seyferts (black solid), composites (blue dotted) and H II region-like galaxies (green dot-dashed). (b) The distribution of $L[\text{OIII}]$ for LINERs (red-dashed), Seyferts (black solid), and H II region-like galaxies (green dot-dashed) where LINERs and Seyferts include LINER+H II and Seyfert+H II composites. (c) $L[\text{OIII}]$ for a uniform random sampling of the Seyferts (black) and LINERs (red), composites (blue) and ambiguous galaxies (purple) as a function of distance from the Ke01 line. (d) The median $L[\text{OIII}]$ for Seyferts (black) and LINERs (red) as a function of distance from the Ke01 line, including Seyfert+H II and LINER+H II galaxies. A distance of 1.0 indicates that the optical line ratios are dominated by ionizing radiation from the Seyfert or LINER nucleus.

D_{SF} for Seyferts, The rise in $L[\text{OIII}]$ implies that the ionizing radiation field is harder for Seyferts with high D_{SF} . Heckman et al. (2005) found that the $L[\text{OIII}]$ and hard X-ray (3-20 keV) luminosities of AGN are correlated over four orders of magnitude.

In LINERs, the median [O III] luminosity falls as a function of D_{SF} until $D_{SF} \sim 0.6$ after which it rises slowly. The drop in $L[\text{OIII}]$ between $D_{SF} \sim 0.6$ occurs where H II+LINER composites are included in the LINER class. The star-formation in these H II+LINER composites is contributing to the [O III] emission until $D_{SF} \sim 0.6$.

5.6 Extinction

In Figure 17 we plot the Balmer decrement for our sample. The median Balmer decrement of LINERs is significantly smaller than for Seyferts, H II region-like galaxies and composites. A substantial fraction (45%) of LINERs have Balmer decrements even less than the theoretical value of 3.1, and 33% of LINERs have Balmer decrements less than the theoretical value for galaxies dominated by star formation (2.86). As discussed in Section 2, a Balmer decrement less than the theoretical value can result from a combination of: (1) intrinsically low reddening, (2) errors in the stellar

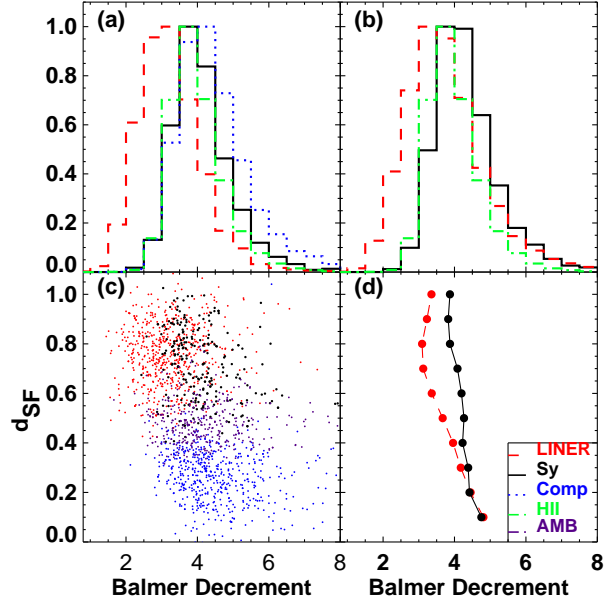


Figure 17. (a) The distribution of the logarithm of the Balmer decrement ($\text{H}\alpha/\text{H}\beta$) for LINERs (red dashed), Seyferts (black solid), composites (blue dotted) and H II region-like galaxies (green dot-dashed). (b) The distribution of $\text{H}\alpha/\text{H}\beta$ for LINERs (red-dashed), Seyferts (black solid), and H II region-like galaxies (green dot-dashed) where LINERs and Seyferts include LINER+H II and Seyfert+H II composites. (c) $\text{H}\alpha/\text{H}\beta$ for a uniform random sampling of the Seyferts (black) and LINERs (red), composites (blue) and ambiguous galaxies (purple) as a function of distance from the Ke01 line. (d) The median $\text{H}\alpha/\text{H}\beta$ for Seyferts (black) and LINERs (red) as a function of distance from the Ke01 line, including Seyfert+H II and LINER+H II galaxies. A distance of 1.0 indicates that the optical line ratios are dominated by ionizing radiation from the Seyfert or LINER nucleus.

absorption correction, and (3) errors in the line flux calibration and measurement. On the other hand, Balmer decrements lower than 3.1 in AGN can indicate a higher nebular temperature (Osterbrock 1989). LINER spectra have strong stellar absorption and errors in the absorption correction could bias the Balmer decrement for LINERs, particularly in spectra with low S/N. We note that many LINERs in our sample have low $\text{H}\beta$ signal-to-noise (S/N) ratios; 11% of Seyferts have $\text{S/N}(\text{H}\beta) < 8$, while 70% of LINERs have $\text{S/N}(\text{H}\beta) < 8$. This low signal-to-noise may cause the low Balmer decrement in some or perhaps most LINERs but it cannot account for the difference for the entire LINER sample because LINERs with high $\text{S/N}(\text{H}\beta) > 8$ have a similar distribution of Balmer decrements to those with lower S/N ratios (Figure 18). Ho et al. (2003) found a similar result for the central few hundred parsecs of Seyferts and LINERs and they suggest that Seyfert galaxies contain nuclear regions that are more gas-rich (and dusty) than LINER galaxies. Our results confirm this conclusion.

The Balmer decrement is not strongly correlated with distance from the star-forming sequence for LINERs (Figure 17b; $r = 0.04$), but it is mildly correlated with d_{SF} for Seyferts ($r = -0.17$ with a formally zero probability of obtaining this value by chance) in the sense that Seyferts

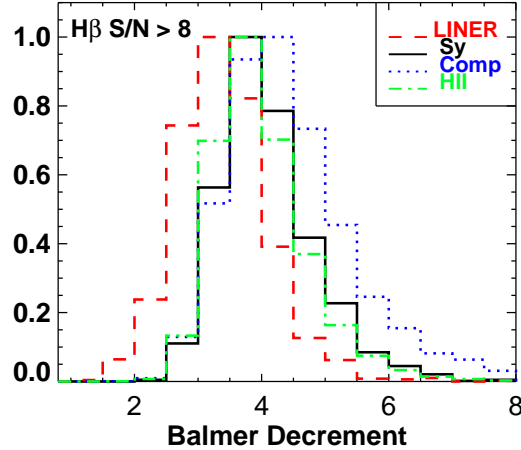


Figure 18. The Balmer decrement distribution for LINERs (red dashed), Seyferts (black solid), composites (blue dotted) and H II region-like galaxies (green dot-dashed) with $S/N(H\beta) > 8$. Even LINERs with high S/N have lower Balmer decrements than the other spectral types.

at large distances from the star-forming sequence contain $\Delta A_V \sim 0.1$ dex less dust on average than Seyferts that are close to the star-forming sequence.

5.7 Host properties across the Seyfert-LINER transition region

Given that many of the host properties of Seyferts and LINERs are substantially different (D4000, $H\delta$, $L[O\text{ III}]$, etc), it is important to understand whether this difference is a truly bimodal distribution or whether the host properties vary smoothly across the Seyfert-LINER dividing line. We define ϕ as the angle to the x-axis in the $[O\text{ III}]/H\beta$ vs $[O\text{ I}]/H\alpha$ diagnostic diagram centered on the blue base point in Figure 2. Therefore LINERs have small ϕ while Seyferts have large ϕ . Figure 19 shows how the host properties of AGN change across the Seyfert-LINER boundary (red dashed lines). The host properties clearly do not form a bimodal distribution; they form a smooth sequence from Seyfert values to LINER values. The correlation coefficients and significance for each panel are given in Table 1. The $L[O\text{ III}]/\sigma^4$ (a proxy for the Eddington ratio) correlates most strongly with ϕ . We will discuss $L[O\text{ III}]/\sigma^4$ as a function of host properties in the following Section.

6 HOST PROPERTIES AS A FUNCTION OF L/L_{EDD}

The accretion rate on the black hole is proportional to the bolometric luminosity of the AGN. The stellar velocity dispersion can be used as an estimate of the black hole mass (Tremaine et al. 2002). In type I Seyferts and quasars, the intrinsic $[O\text{ III}]$ luminosity scales with the AGN bolometric luminosity (see Heckman et al. 2004 for a more detailed discussion). It follows that the quantity $L[O\text{ III}]/\sigma^4$ is proportional to L/L_{EDD} .

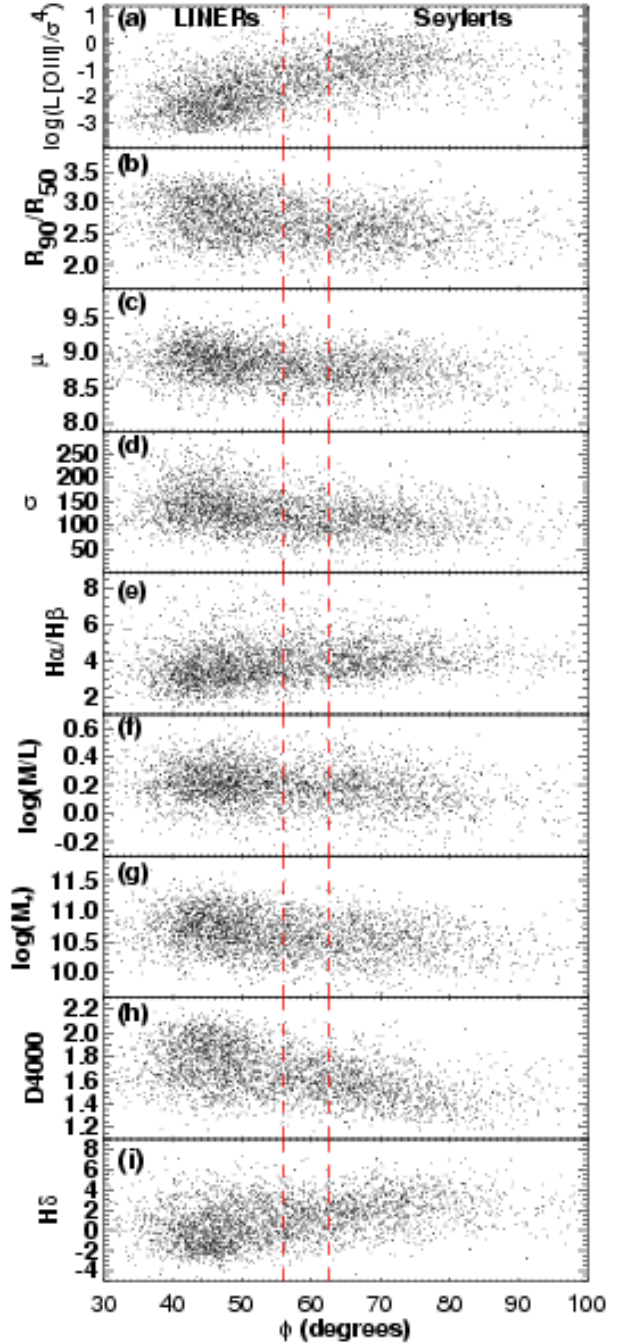


Figure 19. The host galaxy properties as a function of angle ϕ from the x-axis in the $[O\text{ III}]/H\beta$ vs $[O\text{ I}]/H\alpha$ diagnostic diagram. The Seyfert-LINER boundary is shown as red dashed lines. Seyferts lie to the right of the boundary while LINERs lie to the left of the boundary.

In Figure 20 we show that $L[O\text{ III}]/\sigma^4$ does not change as a function of distance from the star-forming sequence for Seyfert galaxies. The $L[O\text{ III}]/\sigma^4$ ratio of LINERs is influenced by star-formation (in $L[O\text{ III}]$) for D_{SF} between 0-0.6, as in Figure 16. Pure Seyferts and LINERs ($D_{SF} \gtrsim 0.6$) have substantially different values of $L[O\text{ III}]/\sigma^4$. Figure 20d in-

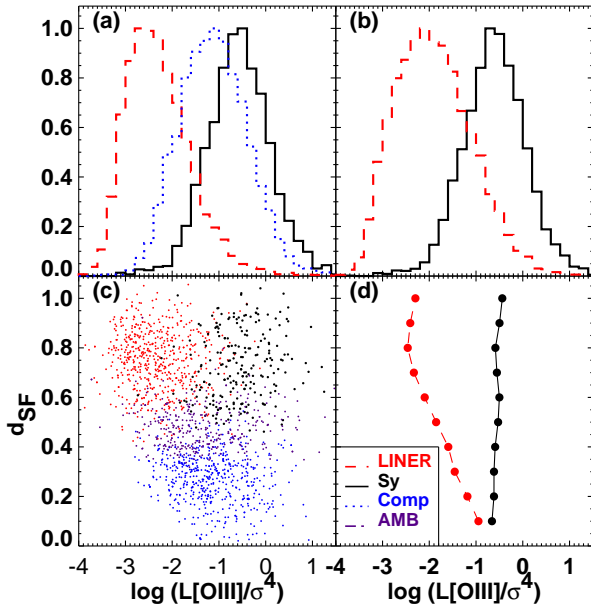


Figure 20. (a) The distribution of the logarithm of $L[\text{OIII}]/\sigma^4$ (corrected for extinction) for LINERs (red dashed), Seyferts (black solid), composites (blue dotted) and H II region-like galaxies (green dot-dashed). (b) The distribution of $L[\text{OIII}]/\sigma^4$ for LINERs (red-dashed), Seyferts (black solid), and H II region-like galaxies (green dot-dashed) where LINERs and Seyferts include LINER+H II and Seyfert+H II composites. (c) $L[\text{OIII}]/\sigma^4$ for Seyferts (black) and LINERs (red), composites (blue) and ambiguous galaxies (purple) as a function of distance from the Ke01 line. (d) $L[\text{OIII}]/\sigma^4$ for Seyferts (black) and LINERs (red) as a function of distance from the Ke01 line, including Seyfert+H II and LINER+H II galaxies. A distance of 1.0 indicates that the optical line ratios are dominated by ionizing radiation from the Seyfert or LINER nucleus.

dicates that $L[\text{OIII}]/\sigma^4$ is roughly constant with D_{SF} for Seyferts. Both $L[\text{OIII}]$ and σ (black hole mass) rise with D_{SF} for Seyferts, resulting in a constant $L[\text{OIII}]/\sigma^4$. The rise in $L[\text{OIII}]$ and σ with D_{SF} probably reflects the trend that older, more massive galaxies contain larger black holes.

We show how the host galaxy properties of LINERs, Seyferts and composites vary as a function of $L[\text{OIII}]/\sigma^4$ in Figure 21. Remarkably, the relationship between $L[\text{OIII}]/\sigma^4$ and all of the host properties for both Seyferts and LINERs forms one smooth sequence. For $L[\text{OIII}]/\sigma^4$ values exhibited by both Seyferts and LINERs ($-1.5 < L[\text{OIII}]/\sigma^4 < -0.5$), the median of the Seyfert and LINER distributions is almost identical for every host property. This result implies that (1) most (if not all) LINERs in our sample are AGN, and that (2) $L[\text{OIII}]/\sigma^4$ is the major fundamental property that divides Seyferts from LINERs and that host property differences are secondary. For example, LINERs are found in larger, older galaxies than Seyferts. Figure 21 shows that the black hole accretion rates are lower in larger, older galaxies and that mass and age do not need to be physically linked to the differences in the LINER and Seyfert emission line spectra.

We check whether a similar effect occurs as a function of $L[\text{OIII}]$ in Figure 22. All of the relations between host properties and $L[\text{OIII}]/\sigma^4$ degrade when $L[\text{OIII}]$ is used in

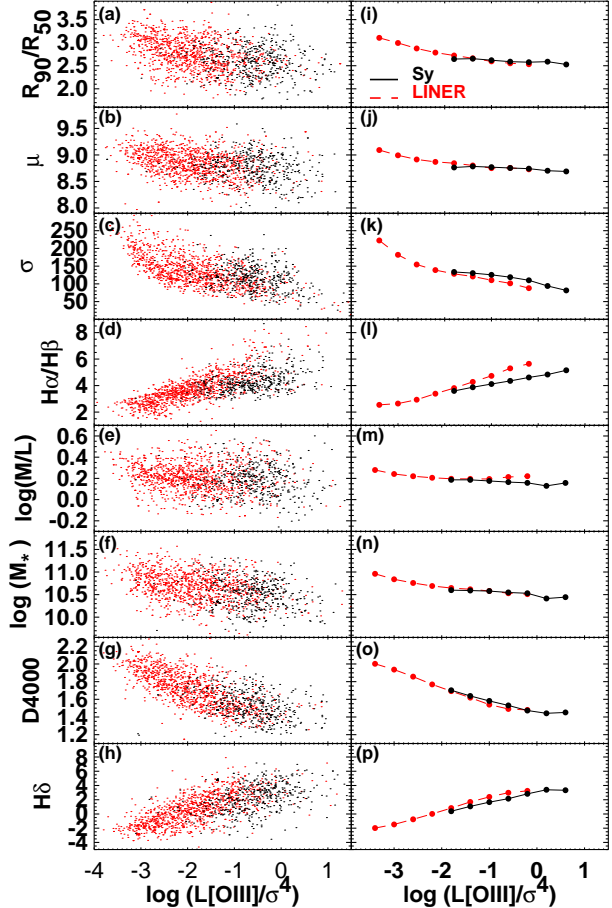


Figure 21. $L[\text{OIII}]/\sigma^4$ versus (a) concentration, (b) surface mass density, (c) stellar velocity dispersion, (d) Balmer decrement, (e) mass-to-light ratio, (f) stellar mass, (g) the D4000 index, and (h) $H\delta$ for LINERs (red), Seyferts (black), and composites (blue). The right panel shows the median values of each host galaxy property for small bins (0.4 dex) of $L[\text{OIII}]/\sigma^4$. Only bins containing more than 150 data points are included.

place of $L[\text{OIII}]/\sigma^4$, confirming that $L[\text{OIII}]/\sigma^4$ is the major property separating Seyferts from LINERs.

7 DISCUSSION

Previous work has shown that almost all normal galaxies contain black holes and black holes appear to evolve with their host galaxies (Ferrarese & Merritt 2000; Gebhardt et al. 2000). In Section 6 we showed that although Seyferts and LINERs display different host properties, these differences are largely resolved when the host properties are considered as a function of $L[\text{OIII}]/\sigma^4$. Thus the strongest difference between Seyferts and LINERs is $L[\text{OIII}]/\sigma^4$, or Eddington ratio. Remarkably, Figure 21 implies that if the Eddington ratio of an AGN is known, then its spectral class and broad host galaxy properties can be deduced.

In Figure 19, we show that the transition in Eddington ratio from Seyferts (high) to LINERs (low) is smooth and that the correlation between classification angle and

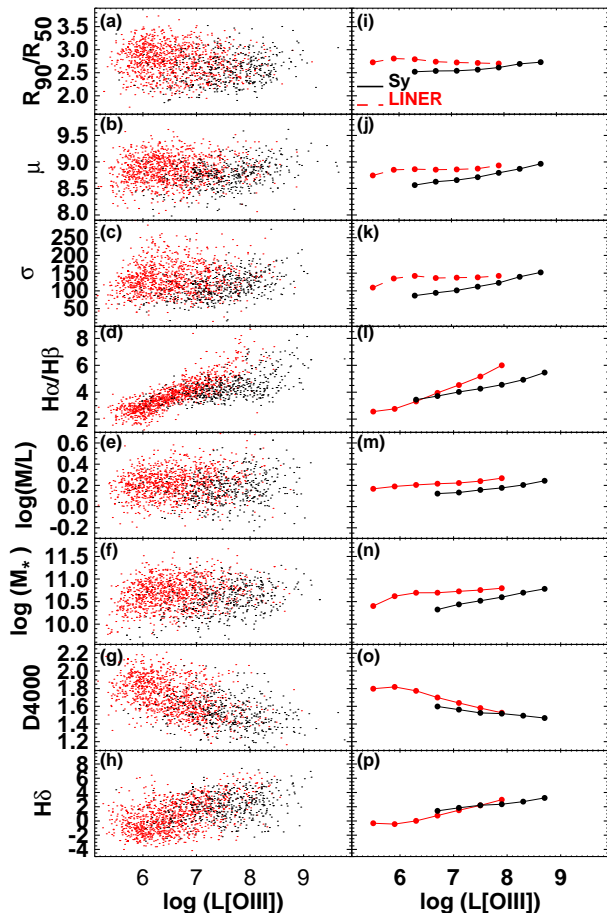


Figure 22. $L[O\text{ III}]$ versus (a) concentration, (b) surface mass density, (c) stellar velocity dispersion, (d) Balmer decrement, (e) mass-to-light ratio, (f) stellar mass, (g) the D4000 index, and (h) $H\delta$ for LINERs (red), Seyferts (black), and composites (blue). The right panel shows the median values of each host galaxy property for small bins (0.4 dex) of $L[O\text{ III}]$. Only bins containing more than 150 data points are included.

$L[O\text{ III}]/\sigma^4$ is stronger than for any of the other host galaxy properties. This Seyfert-LINER transition may be analogous to the transition between high state and low state black hole accretion in X-ray binary systems (e.g., Nowak 1995 and references therein) as suggested by Ho (2005). In X-ray binaries the transition from high to low states is believed to correspond to decreasing mass accretion rates and therefore the primary parameter in many X-ray binary models is the Eddington ratio (e.g., Shakura & Sunyaev 1973; Chen et al. 1995). Theory suggests that an unstable accretion disk may switch between high and low states (Abramowicz et al. 1988; Narayan & Popham 1993; Narayan & Yi 1994, 1995). In this scenario, the energy released by viscous processes in the high state is radiated and the gas is relatively cool. In the low state the viscously released energy may be advected with the gas and radiates inefficiently. This advection dominated accretion flow (ADAF) is stable to thermal and viscous instabilities (Abramowicz et al. 1995; Narayan & Yi 1995). Because the gas loses little energy through radiation in ADAF models, the gas is extremely hot and the weak spectrum pro-

duced is harder than in the high state (e.g., Esin et al. 1997). Alternative scenarios to ADAF models can also produce a weak hard spectrum (Meyer et al. 2000; Ferreira et al. 2006, e.g.). Our observed transition between Seyfert and LINERs occurs at $L[O\text{ III}]/\sigma^4 \sim 0.10$. Assuming a bolometric correction of $L_{\text{BOL}} = 3500L[O\text{ III}]_o$ (Heckman et al. 2004) where $L[O\text{ III}]_o$ is the observed [O III] luminosity, and assuming a mean extinction of $E(B-V) = 0.3$, our Seyfert-LINER transition corresponds to an Eddington ratio of $L/L_{\text{EDD}} \sim 0.05$. This transition L/L_{EDD} is within the range of the observed (and theoretical) transition in X-ray binaries; $0.01 < L/L_{\text{EDD}} < 0.1$ (e.g., Nowak 1995; Narayan 1996; Esin et al. 1997; Barret et al. 2000; Ferreira et al. 2006 and references therein).

We investigate the broad, qualitative differences in radiation field between Seyferts and LINERs using the theoretical AGN photoionization models from MAPPINGS III (Groves et al. 2004a,b). We calculate a simple grid of photoionization models using four power-law indices ($\alpha = -1.2, -1.4, -1.7, -2.0$) and four ionization parameters ($\log(U) = 0, -1.0, -2.0, -3.0$). The MAPPINGS models are self-consistent and include detailed dust physics and radiation pressure. We use a metallicity of $2Z_{\odot}$ and a hydrogen density of 1000 cm^{-3} .

Figure 23 shows the position of our AGN relative to the Seyfert and LINER branches on the $[O\text{ III}]/[O\text{ II}]$ vs $[O\text{ I}]/H\alpha$ diagnostic diagram. The Seyfert branch can be reproduced by an ionizing radiation field with power-law index $\alpha = -1.4$ to -1.8 and a high ionization parameter ($\log(U) = -2.5$ to -1.0). The LINER branch spans a larger range of power-law index, requiring a harder radiation field than Seyferts ($\alpha < -1.4$) at $\log([O\text{ I}]/H\alpha) \geq -0.6$. The LINER branch requires a much lower ionization parameter than the Seyfert branch; the ionization parameter for LINERs ($\log(U) = -3$) is up to an order of magnitude lower than the ionization parameter typical for Seyferts ($\log(U) = -2$ to -2.5). Figure 24 confirms this result and separates ionization parameter from power-law index over a broader range of ionization parameter.

Figures 23 and 24 indicate that the hardness of the ionizing radiation field increases as a function of distance from the star-forming sequence. We know that Seyferts contain a young-intermediate age stellar population (Figures 11, 12) and that both Seyfert-H II and LINER-composites exist. Given these results, one would expect that the stellar emission would be overwhelmed by the luminous Seyfert emission in Seyfert-H II composites but that stellar emission could dominate in many LINER-H II composites. In this case, there should be many more LINER-H II composites than Seyfert-H II composites. The fact that the Seyfert to LINER ratio is independent of d_{SF} (Figure 10) implies that star formation and AGN are coupled in Seyfert galaxies such that more powerful AGN also have stronger star formation. Further theoretical and observational work are required to confirm this connection between star formation and Seyfert emission.

8 CONCLUSIONS

We have analyzed the emission-line and host properties of 85224 galaxies from the Sloan Digital Sky Survey. We show that Seyferts and LINERs form two separate branches on the standard optical diagnostic diagrams. We present a

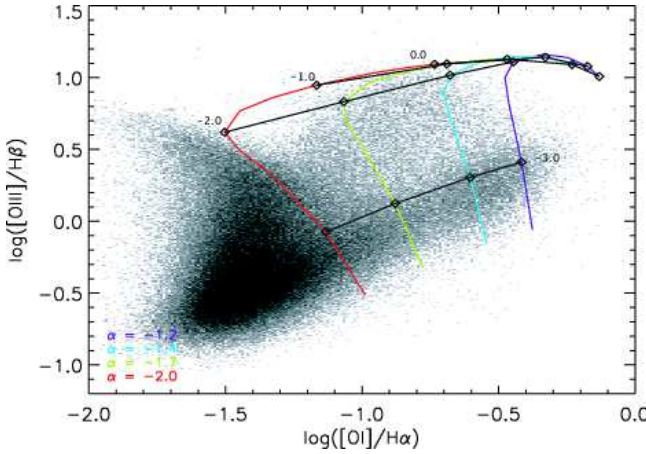


Figure 23. The $[\text{O III}]/\text{H}\beta$ vs $[\text{O I}]/\text{H}\alpha$ diagnostic diagram showing the SDSS galaxies (black points) and our theoretical dusty radiation pressure dominated AGN models. These models were calculated assuming a metallicity of $2Z_\odot$ and a hydrogen density of 1000 cm^{-3} . The model grids are given for four ionization parameters ($\log(U) = 0, -1, -2, -3$) and four power-law indices ($\alpha = -1.2, -1.4, -1.7, -2.0$) as marked. The radiation field in LINERs requires a lower ionization parameter than in Seyfert galaxies and LINERs with strong $[\text{O I}]/\text{H}\alpha$ require a harder radiation field than Seyferts.

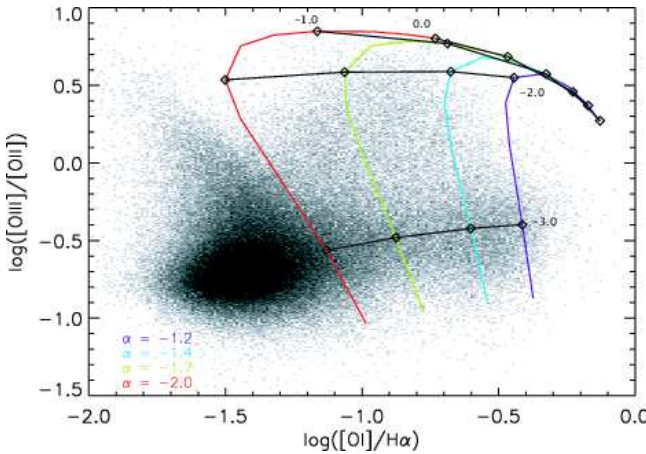


Figure 24. The $[\text{O III}]/[\text{O II}]$ vs $[\text{O I}]/\text{H}\alpha$ diagnostic diagram showing the SDSS galaxies (black points) and our theoretical dusty radiation pressure dominated AGN models. These models were calculated assuming a metallicity of $2Z_\odot$ and a hydrogen density of 1000 cm^{-3} . The model grids are given for four ionization parameters ($\log(U) = 0, -1, -2, -3$) and four power-law indices ($\alpha = -1.2, -1.4, -1.7, -2.0$) as marked. The radiation field in LINERs requires a lower ionization parameter than in Seyfert galaxies and LINERs with strong $[\text{O I}]/\text{H}\alpha$ require a harder radiation field than Seyferts.

new optical classification scheme that successfully separates purely star-forming galaxies, Seyferts, LINERs, and composite AGN+star-forming galaxies. We show that $[\text{O III}]/[\text{O II}]$ vs $[\text{O I}]/\text{H}\alpha$ diagnostic diagram easily discriminates between Seyferts, LINERs and galaxies dominated by star-formation (including composites). We use our new classification scheme to investigate the host properties of AGN galaxies as a function of distance from the star-forming sequence. We find that:

- The ratio of Seyferts to LINERs is invariant with distance from the star-forming sequence. This result implies that star formation and AGN power are coupled.

• The stellar populations of Seyferts and LINERs age with distance from the star-forming sequence. LINERs have a substantially older stellar population than the other spectral types. The youngest stellar population in LINERs has $D4000$ and $H\delta$ values consistent with the oldest stellar population in Seyferts on average.

- The stellar mass and mass-to-light ratios of Seyferts and LINERs are not strongly correlated with distance from the star-forming sequence. However, LINERs have slightly higher stellar masses and mass-to-light ratios on average than Seyferts or composite objects.

We use $L[\text{O III}]/\sigma^4$ as an indicator of the accretion rate in Eddington units. We compare the host properties of Seyfert and LINER galaxies as a function of $L[\text{O III}]$ and $L[\text{O III}]/\sigma^4$. We show that:

- The strongest difference between Seyfert and LINER galaxies is $L[\text{O III}]/\sigma^4$.
- When the host properties of Seyferts and LINERs are considered in terms of $L[\text{O III}]/\sigma^4$, the differences in host properties is resolved and the host properties of Seyferts and LINERs form a smooth sequence with $L[\text{O III}]/\sigma^4$.
- When the host properties of Seyferts and LINERs are considered in terms of $L[\text{O III}]$, the smooth sequence seen with $L[\text{O III}]/\sigma^4$ disappears.

These results indicate that most (if not all) LINERs contain AGN, and that the major fundamental difference between Seyferts and LINERs is accretion rate. We use theoretical AGN photoionization models to show that the LINER branch requires a lower ionization parameter (up to an order of magnitude) than the Seyfert branch, and that strong LINERs ($\log([\text{O I}]/\text{H}\alpha) > -1.6$) require a harder ionizing radiation field than galaxies on the Seyfert branch. These results suggest that the transition between Seyferts and LINERs is analogous to the high-state and low-state transition in X-ray binaries.

ACKNOWLEDGMENTS

L. J. Kewley is supported by a Hubble Fellowship. This research has made use of NASA's Astrophysics Data System Bibliographic Services.

Funding for the creation and distribution of the SDSS Archive has been provided by the Alfred P. Sloan Foundation, the Participating Institutions, the National Aeronautics and Space Administration, the National Science Foundation, the U.S. Department of Energy, the Japanese Monbukagakusho, and the Max Planck Society. The SDSS Web site is <http://www.sdss.org/>.

The SDSS is managed by the Astrophysical Research Consortium (ARC) for the Participating Institutions. The Participating Institutions are The University of Chicago, Fermilab, the Institute for Advanced Study, the Japan Participation Group, The Johns Hopkins University, Los Alamos National Laboratory, the Max-Planck-Institute for Astronomy (MPIA), the Max-Planck-Institute for Astrophysics (MPA), New Mexico State University, University of

Pittsburgh, Princeton University, the United States Naval Observatory, and the University of Washington.

REFERENCES

Abramowicz, M. A., Chen, X., Kato, S., Lasota, J.-P., & Regev, O. 1995, *ApJL*, 438, L37

Abramowicz, M. A., Czerny, B., Lasota, J. P., & Szuszkiewicz, E. 1988, *ApJ*, 332, 646

Alonso-Herrero, A., Rieke, M. J., Rieke, G. H., & Shields, J. C. 2000, *ApJ*, 530, 688

Anderson, J. M., Ulvestad, J. S., & Ho, L. C. 2004, *ApJ*, 603, 42

Baldwin, J. A., Phillips, M. M., & Terlevich, R. 1981, *PASP*, 93, 5

Balogh, M. L., Morris, S. L., Yee, H. K. C., Carlberg, R. G., & Ellingson, E. 1999, *ApJ*, 527, 54

Barret, D., Olive, J. F., Boirin, L., Done, C., Skinner, G. K., & Grindlay, J. E. 2000, *ApJ*, 533, 329

Barth, A. J., & Shields, J. C. 2000, *PASP*, 112, 753

Bower, G. A., Wilson, A. S., Heckman, T. M., & Richstone, D. O. 1996, *AJ*, 111, 1901

Bruzual, G., & Charlot, S. 2003, *MNRAS*, 344, 1000

Bruzual A., G. 1983, *ApJ*, 273, 105

Cardelli, J. A., Clayton, G. C., & Mathis, J. S. 1989, *ApJ*, 345, 245

Cecil, G., Greenhill, L. J., DePree, C. G., Nagar, N., Wilson, A. S., Dopita, M. A., Pérez-Fournon, I., Argon, A. L., & Moran, J. M. 2000, *ApJ*, 536, 675

Chen, X., Abramowicz, M. A., Lasota, J.-P., Narayan, R., & Yi, I. 1995, *ApJL*, 443, L61

Colina, L., Gonzalez Delgado, R., Mas-Hesse, J. M., & Leitherer, C. 2002, *ApJ*, 579, 545

Denicoló, G., Terlevich, R., & Terlevich, E. 2002, *MNRAS*, 330, 69

Dopita, M. A., & Sutherland, R. S. 1995, *ApJ*, 455, 468

Drory, N., Salvato, M., Gabasch, A., Bender, R., Hopp, U., Feulner, G., & Pannella, M. 2005, *ApJL*, 619, L131

Eracleous, M., & Halpern, J. P. 2001, *ApJ*, 554, 240

Esin, A. A., McClintock, J. E., & Narayan, R. 1997, *ApJ*, 489, 865

Falcke, H., Nagar, N. M., Wilson, A. S., & Ulvestad, J. S. 2000, *ApJ*, 542, 197

Fernandes, R. C., Delgado, R. M. G., Schmitt, H., Storchi-Bergmann, T., Martins, L. P., Pérez, E., Heckman, T., Leitherer, C., & Schaerer, D. 2004, *ApJ*, 605, 105

Ferrarese, L., & Merritt, D. 2000, *ApJL*, 539, L9

Ferreira, J., Petrucci, P.-O., Henri, G., Saugé, L., & Pelletier, G. 2006, *A&A*, 447, 813

Filho, M. E., Barthel, P. D., & Ho, L. C. 2002, *A&A*, 385, 425

Filho, M. E., Fraternali, F., Markoff, S., Nagar, N. M., Barthel, P. D., Ho, L. C., & Yuan, F. 2004, *A&A*, 418, 429

Filippenko, A. V., & Terlevich, R. 1992, *ApJL*, 397, L79

Gallazzi, A., Charlot, S., Brinchmann, J., White, S. D. M., & Tremonti, C. A. 2005, *MNRAS*, 362, 41

Gebhardt, K., Bender, R., Bower, G., Dressler, A., Faber, S. M., Filippenko, A. V., Green, R., Grillmair, C., Ho, L. C., Kormendy, J., Lauer, T. R., Magorrian, J., Pinkney, J., Richstone, D., & Tremaine, S. 2000, *ApJL*, 539, L13

González Delgado, R. M., Cid Fernandes, R., Pérez, E., Martins, L. P., Storchi-Bergmann, T., Schmitt, H., Heckman, T., & Leitherer, C. 2004, *ApJ*, 605, 127

González Delgado, R. M., Heckman, T., Leitherer, C., Meurer, G., Krolik, J., Wilson, A. S., Kinney, A., & Koratkar, A. 1998, *ApJ*, 505, 174

González Delgado, R. M., Leitherer, C., & Heckman, T. M. 1999, *ApJS*, 125, 489

Gorgas, J., Cardiel, N., Pedraz, S., & González, J. J. 1999, *A&As*, 139, 29

Groves, B. A., Dopita, M. A., & Sutherland, R. S. 2004a, *ApJS*, 153, 9

—. 2004b, *ApJS*, 153, 75

Heckman, T. M. 1980, *A&A*, 87, 152

Heckman, T. M., Gonzalez-Delgado, R., Leitherer, C., Meurer, G. R., Krolik, J., Wilson, A. S., Koratkar, A., & Kinney, A. 1997, *ApJ*, 482, 114

Heckman, T. M., Kauffmann, G., Brinchmann, J., Charlot, S., Tremonti, C., & White, S. D. M. 2004, *ApJ*, 613, 109

Heckman, T. M., Ptak, A., Hornschemeier, A., & Kauffmann, G. 2005, *ApJ*, 634, 161

Heckman, T. M., van Breugel, W., Miley, G. K., & Butcher, H. R. 1983, *AJ*, 88, 1077

Ho, L. C. 2005, *Ap&SS*, 300, 219

Ho, L. C., Feigelson, E. D., Townsley, L. K., Sambruna, R. M., Garmire, G. P., Brandt, W. N., Filippenko, A. V., Griffiths, R. E., Ptak, A. F., & Sargent, W. L. W. 2001, *ApJL*, 549, L51

Ho, L. C., Filippenko, A. V., & Sargent, W. L. 1995, *ApJS*, 98, 477

Ho, L. C., Filippenko, A. V., & Sargent, W. L. W. 1997a, *ApJS*, 112, 315

—. 1997b, *ApJ*, 487, 568

—. 2003, *ApJ*, 583, 159

Kauffmann, G., Heckman, T. M., Tremonti, C., Brinchmann, J., Charlot, S., White, S. D. M., Ridgway, S. E., Brinkmann, J., Fukugita, M., Hall, P. B., Ivezić, Ž., Richards, G. T., & Schneider, D. P. 2003a, *MNRAS*, 346, 1055

Kauffmann, G., Heckman, T. M., White, S. D. M., Charlot, S., Tremonti, C., Brinchmann, J., Bruzual, G., Peng, E. W., Seibert, M., Bernardi, M., Blanton, M., Brinkmann, J., Castander, F., Csabai, I., Fukugita, M., Ivezić, Ž., Munn, J. A., Nichol, R. C., Padmanabhan, N., Thakar, A. R., Weinberg, D. H., & York, D. 2003b, *MNRAS*, 341, 33

Kauffmann, G., Heckman, T. M., White, S. D. M., Charlot, S., Tremonti, C., Brinchmann, J., Bruzual, G., Peng, E. W., Seibert, M., Bernardi, M., Blanton, M., Brinkmann, J., Castander, F., Csabai, I., Fukugita, M., Ivezić, Ž., Munn, J. A., Nichol, R. C., Padmanabhan, N., Thakar, A. R., Weinberg, D. H., & York, D. 2003c, *MNRAS*, 341, 33

Kewley, L. J., & Dopita, M. A. 2002, *ApJS*, 142, 35

Kewley, L. J., Dopita, M. A., Sutherland, R. S., Heisler, C. A., & Trevena, J. 2001a, *ApJ*, 556, 121

Kewley, L. J., Heisler, C. A., Dopita, M. A., & Lumsden, S. 2001b, *ApJS*, 132, 37

Kewley, L. J., Jansen, R. A., & Geller, M. J. 2005, *PASP*, 117, 227

Lípari, S., Mediavilla, E., García-Lorenzo, B., Díaz, R. J., Acosta-Pulido, J., Agüero, M. P., Taniguchi, Y., Dottori,

H., & Terlevich, R. 2004, MNRAS, 355, 641

Maoz, D., Koratkar, A., Shields, J. C., Ho, L. C., Filippenko, A. V., & Sternberg, A. 1998, AJ, 116, 55

Maoz, D., Nagar, N. M., Falcke, H., & Wilson, A. S. 2005, ApJ, 625, 699

Meyer, F., Liu, B. F., & Meyer-Hofmeister, E. 2000, A&A, 354, L67

Narayan, R. 1996, ApJ, 462, 136

Narayan, R., & Popham, R. 1993, Nature, 362, 820

Narayan, R., & Yi, I. 1994, ApJL, 428, L13

—. 1995, ApJ, 452, 710

Nowak, M. A. 1995, PASP, 107, 1207

Osterbrock, D. E. 1989, Astrophysics of gaseous nebulae and active galactic nuclei (Research supported by the University of California, John Simon Guggenheim Memorial Foundation, University of Minnesota, et al. Mill Valley, CA, University Science Books, 1989, 422 p.)

Osterbrock, D. E., & Pogge, R. W. 1985, ApJ, 297, 166

Pettini, M., & Pagel, B. E. J. 2004, MNRAS, 348, L59

Shakura, N. I., & Sunyaev, R. A. 1973, A&A, 24, 337

Shields, J. C. 1992, ApJL, 399, L27

Spergel, D. N., Verde, L., Peiris, H. V., Komatsu, E., Nolta, M. R., Bennett, C. L., Halpern, M., Hinshaw, G., Jarosik, N., Kogut, A., Limon, M., Meyer, S. S., Page, L., Tucker, G. S., Weiland, J. L., Wollack, E., & Wright, E. L. 2003, ApJS, 148, 175

Storchi-Bergmann, T., Eracleous, M., Ruiz, M. T., Livio, M., Wilson, A. S., & Filippenko, A. V. 1997, ApJ, 489, 87

Taniguchi, Y., Shioya, Y., & Murayama, T. 2000, AJ, 120, 1265

Terashima, Y., Ho, L. C., & Ptak, A. F. 2000, ApJ, 539, 161

Tremaine, S., Gebhardt, K., Bender, R., Bower, G., Dressler, A., Faber, S. M., Filippenko, A. V., Green, R., Grillmair, C., Ho, L. C., Kormendy, J., Lauer, T. R., Magorrian, J., Pinkney, J., & Richstone, D. 2002, ApJ, 574, 740

Tremonti, C. A., Heckman, T. M., Kauffmann, G., Brinchmann, J., Charlot, S., White, S. D. M., Seibert, M., Peng, E. W., Schlegel, D. J., Uomoto, A., Fukugita, M., & Brinkmann, J. 2004, ApJ, 613, 898

Ulvestad, J. S., & Ho, L. C. 2001, ApJL, 562, L133

Veilleux, S., & Osterbrock, D. E. 1987, ApJS, 63, 295

Worthey, G., & Ottaviani, D. L. 1997, ApJS, 111, 377

Table 1. Correlation Coefficients

Figure	x-axis	y-axis	corr. coeff ¹	prob ² (%)
10	Sy/L ratio	d_{SF}	-0.36	31
11c (LINERs)	D4000	d_{SF}	0.74	0.0 ³
11c (Seyferts)	D4000	d_{SF}	0.45	0.0 ³
12c (LINERs)	$H\delta_A$	d_{SF}	-0.67	0.0 ³
12c (Seyferts)	$H\delta_A$	d_{SF}	-0.32	0.0 ³
13c (LINERs)	$\log(M_*)$	d_{SF}	0.25	0.0 ³
13c (Seyferts)	$\log(M_*)$	d_{SF}	0.11	1×10^{-13}
14c (LINERs)	$\log(M/L)$	d_{SF}	0.10	0.0 ³
14c (Seyferts)	$\log(M/L)$	d_{SF}	0.12	1×10^{-14}
15c (LINERs)	σ_*	d_{SF}	0.45	0.0 ³
15c (Seyferts)	σ_*	d_{SF}	0.20	0.0 ³
16c (LINERs)	$\log(L([OIII]))$	d_{SF}	-0.13	0.0 ³
16c (Seyferts)	$\log(L([OIII]))$	d_{SF}	0.38	0.0 ³
17c (LINERs)	$H\alpha/H\beta$	d_{SF}	-0.48	24
17c (Seyferts)	$H\alpha/H\beta$	d_{SF}	-0.23	24
20c (LINERs)	$\log(L([OIII])/\sigma^4)$	d_{SF}	-0.50	0.0 ³
20c (Seyferts)	$\log(L([OIII])\sigma^4)$	d_{SF}	0.07	6×10^{-6}
19a	ϕ	$\log(L([OIII])/\sigma^4)$	0.51	0.0 ³
19b	ϕ	R_{90}/R_{50}	-0.27	0.0 ³
19c	ϕ	μ	-0.28	0.0 ³
19d	ϕ	σ	-0.33	0.0 ³
19e	ϕ	$H\alpha/H\beta$	0.28	0.0 ³
19f	ϕ	$\log(M/L)$	-0.21	0.0 ³
19g	ϕ	$\log(M_*)$	-0.30	0.0 ³
19h	ϕ	D4000	-0.46	0.0 ³
19i	ϕ	D4000	0.37	0.0 ³

¹ Spearman-Rank correlation coefficient² Probability of obtaining the correlation coefficient value by chance³ Probability of obtaining the correlation coefficient value by chance is formally zero ($1 \times 10^{-29}\%$)